Future Köppen-Geiger Climate Zones over Southeast Asia using CMIP6 Multimodel Ensemble

Mohammed Magdy Hamed[1,2,*] eng.mohammedhamed@aast.edu, Mohamed Salem Nashwan[3] m.salem@aast.edu, Shamsuddin Shahid[2], Xiao-jun Wang[4,5] xjwang@nhri.cn, Tarmizi bin Ismail[2], Ashraf Dewan[6] A.Dewan@curtin.edu.au, Md Asaduzzaman[7] Md.Asaduzzaman@staffs.ac.uk

[1]Construction and Building Engineering Department, College of Engineering and Technology, Arab Academy for Science, Technology and Maritime Transport (AASTMT), B 2401 Smart Village, 12577, Giza, Egypt

[2]Department of Water and Environmental Engineering, School of Civil Engineering, Faculty of Engineering, Universiti Teknologi Malaysia (UTM), 81310 Skudia, Johor, Malaysia

[3]Construction and Building Engineering Department, College of Engineering and Technology, Arab Academy for Science, Technology and Maritime Transport (AASTMT), 2033 Elhorria, Cairo, Egypt

[4]State Key Laboratory of Hydrology-Water Resources and Hydraulic Engineering, Nanjing Hydraulic Research Institute, Nanjing 210029, China

[5]Research Center for Climate Change, Ministry of Water Resources, Nanjing 210029, China.

[6]Spatial Sciences Discipline, School of Earth and Planetary Sciences, Curtin University, Kent Street, Bentley, Perth 6102, Australia.

[7]Department of Engineering, School of Digital, Technologies and Arts, Staffordshire University, Stoke-on-Trent, UK.

[*]Corresponding author.

Abstract

A possible shift in climate zones in Southeast Asia (SEA) for different shared socioeconomic pathways (SSPs) is evaluated in this study. The ability of 19 Coupled Model Intercomparison Project (CMIP6) global climate models (GCMs) in reconstructing the Köppen-Geiger climate zones in SEA, estimated using reanalysis data (ERA5) for the period 1979–2014, was analysed using five categorical evaluation metrics. The best-performing models were selected to prepare an ensemble to project possible shifts in climate zones for different SSP scenarios in the future. Besides, future projections in climate variables were evaluated to assess the driving factor of climate shifts in the future. The results showed that three CMIP6 GCMs, EC-Earth3-Veg-LR, CMCC-ESM2 and CanESM5, had a higher skill in classifying the observed climate of SEA. Selected GCMs showed climate shifting in 3.4 to 12.6% of the total area of SEA for different SSPs. The highest geographical shift in climate was projected in the north, from dry winter and hot summer (Cwa) to tropical with dry winter (Aw), followed by Aw to tropical monsoon (Am) in the north and south, and tropical without dry season (Af) to Am in the middle and southwest of SEA. An increase in minimum temperature was the key to climate shifting from Cwa to Aw in the north, while increased rainfall was a reason for Aw to Am transition in the north and south. Overall, climatic shifting was higher for high emission scenarios. The maps of future climate zones generated in this study can help to identify the hotspots of ecologically vulnerable areas in SEA due to climate change.

Keywords

Köppen-Geiger climate classification, global climate models, shared socioeconomic pathways, spatial metrics, climate shifts

1. Introduction

Extensive changes in the world's climatic systems due to increased human activities have caused an increase in global mean temperature, causing spatiotemporal changes in rainfall (IPCC, 2018). It has been projected that the hydrological cycle will become more intense. As a result, the greater difference between wet and dry places could be highly pronounced (Hartmann et al., 2013). Because of uneven changes in climate, some regions of Earth's surface would suffer big changes than its surroundings. The shifting in climatic variables is likely to change ecology (Chen et al., 2011; Parmesan, 2006), water systems (Taylor et al., 2013; Zhang and Cai, 2013), food supply chain (Lobell and Gourdji, 2012) and natural forestation (Karl et al., 2009). Due to climate shifts, the reorganisation of the present distribution of animals and plants may potentially affect social and agricultural systems, which could be pervasive and long-lasting. It may also severely affect biodiversity (Cui et al., 2021a). Therefore, there is a growing need to quantify the effects of climate change on the Earth's terrestrial bioclimate.

Studies revealed a significant shift in the regional climate in different regions of the globe (Belda et al., 2014; Rohli et al., 2015). Cui et al. (2021a) showed that over 5% of the total global land had experienced a climate shift in the last 40 years. Around a quarter of the global land would experience a further shift by the end of this century under RCP8.5. However, the studies suggested a more precise portrayal of climatic conditions for various projection scenarios and extended temporal coverage is needed to accurately detect future land shifting to different climate zones (Bickford et al., 2010; Holbourn et al., 2018; Kim and Bae, 2021).

Traditional metrics are generally used in previous studies to identify temporal climatic shifts in an area. For instance, Loarie et al. (2009) utilised the shift velocity of isotherms to characterise changes in climatic conditions. Williams et al. (2007) used a formulation based on Euclidean distance that merges rainfall and temperature parameters to understand changes in climate classification of a given area. Besides, many researchers evaluated climate classification and shifting based on different techniques such as clustering (Netzel and Stepinski, 2016), correlation (Hubalek and Horakova, 1988), climate mapping (Holdridge, 1947; Walter and Elwood, 1975) and dynamic time warping (Netzel and Stepinski, 2017). Köppen's climate classification is widely used to identify spatial patterns of climates based on monthly rainfall and temperature (Köppen, 1936). Several studies have used Köppen categorisation schemes to assess changes in climate zonation due to probable climate (Belda

et al., 2016, 2014; Cui et al., 2021b, 2021a; Kottek et al., 2006; Kriticos et al., 2012; Peel et al., 2007; Rohli et al., 2015). Fernandez et al. (2017) used Köppen-Trewartha to understand possible climate shifting in South America using historical and projected climate, based on regional climate models. Beck et al. (2018) generated the world's future Köppen climate classification map for different radiative concentration pathways (RCPs).

The global climate models of Coupled Model Intercomparison Project (CMIP6) provide climate projections for new scenarios, the shared socioeconomic pathways (SSPs) (Moss et al., 2010; Schlund et al., 2020; Taylor et al., 2012). CMIP6 GCMs are distinct from previous CMIPs in that version 6 gives a more realistic representation of Earth's physical processes (Gusain et al., 2020). These updated scenarios take socioeconomic improvements, technological advancement, and additional environmental aspects such as land use to project future climate (Eyring et al., 2016). The release of CMIP6 urges climate change impact assessment using climate projections for new scenarios.

Southeast Asia (SEA) is globally the most vulnerable region to climate change (Raitzer et al., 2015; Vinke et al., 2017). The mean temperature in SEA has risen by 0.1 °C/decade during the previous 50 years (IPCC, 2007). In addition, extreme weather events in the region showed significant fluctuations over time (Nasional BPP 2012). GCM simulations showed a temperature rise of 1.99 °C and 4.25 °C for SSP 4.5 and 8.5 by the end of the century (Supharatid and Nafung, 2021). Besides, climate change is anticipated to increase the frequency of extremes in the future, putting SEA at risk of ramifications (Ge et al., 2019). This has made four SEA countries among the ten top climate hotspots of the globe (Harmeling and Eckstein, 2013). A recent study showed that SEA's gross domestic product (GDP) would be reduced by 11% at the end of the present century due to climate change (Raitzer et al., 2015). Agriculture and ecological services are believed to experience devastating impacts (Li et al., 2014; Valentin et al., 2008; Zhao et al., 2006). There would be a significant decline in crop yield due to the heating of the land surface in a changing climate (Tomaszkiewicz, 2021). A significant biome shift might affect millions' ecosystems and livelihoods (Woetzel et al., 2020). Evaluation of a possible shift in climate zones over SEA is, therefore, crucial to the sustainable development of the region (Bickford et al., 2010; Holbourn et al., 2018; Kim and Bae, 2021).

SEA climate simulations have proven difficult due to the difficult land-ocean border and irregular spatial variability, especially when utilising coarse resolution GCMs (Robertson et

al., 2011). Projections of CMIP6 GCMs are also prone to uncertainty (Almazroui et al., 2020; Deng et al., 2021; Ombadi et al., 2020), which is largely owing to insufficient model explanations of the physical processes controlling the climate system and climatic scenarios (Weigel et al., 2010). An ensemble of GCMs is generally used to reduce uncertainties linked with their projections (Chhin and Yoden, 2018). Many researchers also suggested making an ensemble of GCMs depending on their ability to replicate observed climate to minimise uncertainty in climate projection (Jiang et al., 2015; Lutz et al., 2016; Ahmed et al., 2019; Hamed et al., 2022a).

This research aims to evaluate a possible shift in climatic zones in SEA under different SSPs and future periods. The ability of GCMs to replicate the geographical extents of the present climate classes is evaluated to select the GCMs. An ensemble mean of the GCMs is employed to estimate a possible shift in climate zones in the future. This is the first attempt to select the most suitable CMIP6 GCMs that replicated the Köppen-Geiger climate classification in SEA. Besides, uncertainty in climate shifting is evaluated to provide information on possible spatial extents of the shifts in upper and lower limits. The novelty of this study is the use of readily available future climate zones maps to provide an understanding of the possible shift in climate. The maps generated in this study can also be used to identify the ecologically vulnerable areas in SEA due to climate change for further studies for developing effective climate change mitigation and adaptation measures.

2. Data

2.1. Study area

SEA is made up of ten sovereign members of the Association of Southeast Asian Nations (ASEAN) and Timor-Leste. The region's total population is 563 million, with a land area of 4,330,079 km^2 (Fig. 1). It has 173,251 km of coastline. SEA is one of the world's most vulnerable regions to the effects of climate change due to its unique geographic and climatic circumstances and demographic, economic, and social conditions. SEA comprises oceans, lands and islands spread across eleven nations. The region is divided into two major areas, i.e., Mainland and Maritime Southeast Asia. Except for Myanmar and Indonesia, where elevation can be more than 4000 m above sea level, SEA is largely a flat landscape. The region's average temperature is 25 °C, while the mean annual rainfall varies between 750 and

5000 mm (Peel et al., 2007; Yang et al., 2021). Climate-related disasters have occurred at different spatiotemporal scales, such as floods, droughts and other weather-related disruptions (Kuo et al., 2020; Mukherjee et al., 2018). SEA is classified as tropical and warm temperature zones based on the Köppen-Geiger climate classification (Kim and Bae, 2021). The tropical rainforest climate (Af) covered around 47% of the total area, with a temperature higher than 18 ℃. Large-scale ocean-atmospheric phenomena such as Madden-Julian Oscillation (MJO), the El Nino-Southern Oscillation (ENSO), equatorial waves, Cross-Equatorial Northerly Surge (CENS) and the Indian Ocean Dipole (IOD) had significant impacts on the amount and extreme rainfall events over SEA (Harjupa et al., 2022; Hattori et al., 2011; Xavier et al., 2014).

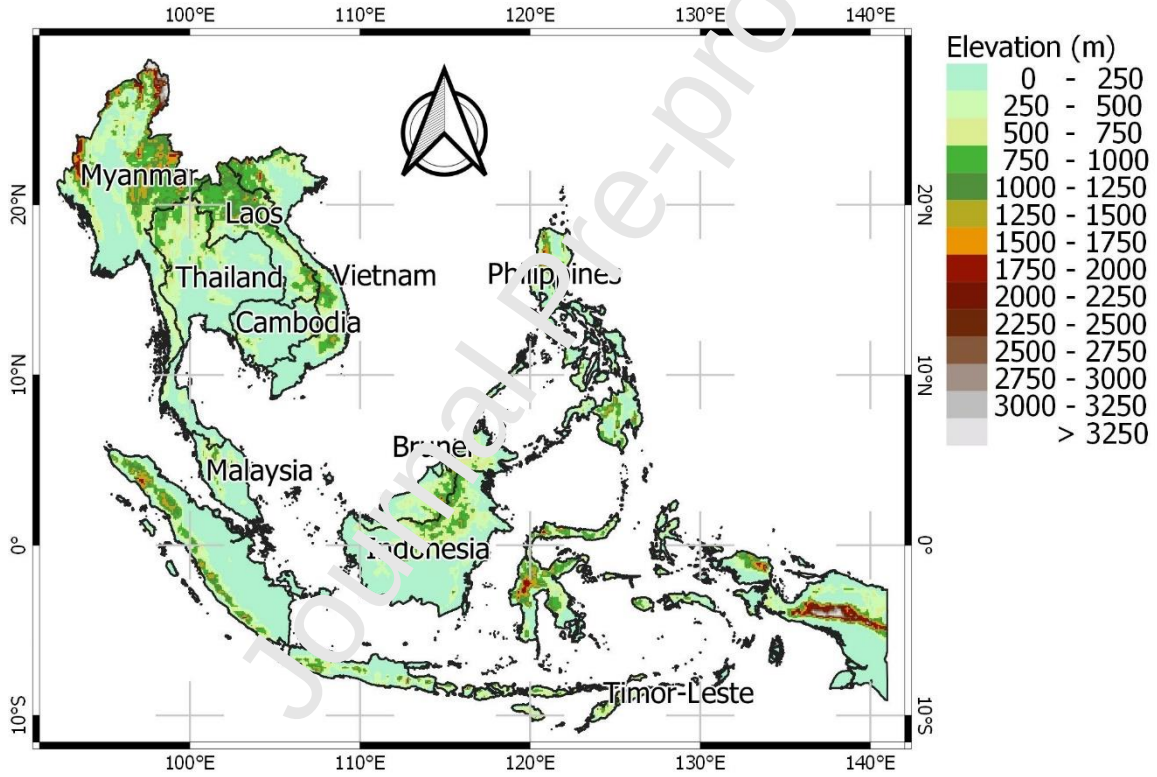

Fig. 1 The location and topography of Southeast Asia

2.2. Reanalysis gridded rainfall and temperature datasets

The European Centre for Medium-Range Weather Forecasts (ECMWF) has issued its fifth atmospheric, oceanic, and land-surface reanalysis product, ERA5 (Hersbach et al., 2020). The Integrated Forecasting System (IFS) cycle 41r2 was improved by including high-quality global data to develop ERA5. This study employed ERA5 monthly cumulative rainfall and

monthly average T_{max} and T_{min} datasets with a 0.25-degree resolution, spanning from January 1979 to December 2014. Fig. 2 depicts the spatial distribution of mean annual rainfall, T_{max} and T_{min} over SEA. The maximum annual rainfall (>5000 mm) occurs in the Hkakabo Razi Mountains in the north and Papua in the south, with a heterogeneous distribution of T_{max} and T_{min}. Contrarily, the lowest rainfall takes place in the middle of Myanmar (Fig. 2a). Both T_{max} (Fig. 2b) and T_{min} (Fig. 2c) exhibit the lowest values at the Hkakabo Razi Mountains to the north with 4 and -4 °C, respectively. High T_{max} (~34 °C) occurs in Thailand and Cambodia (Fig. 2b).

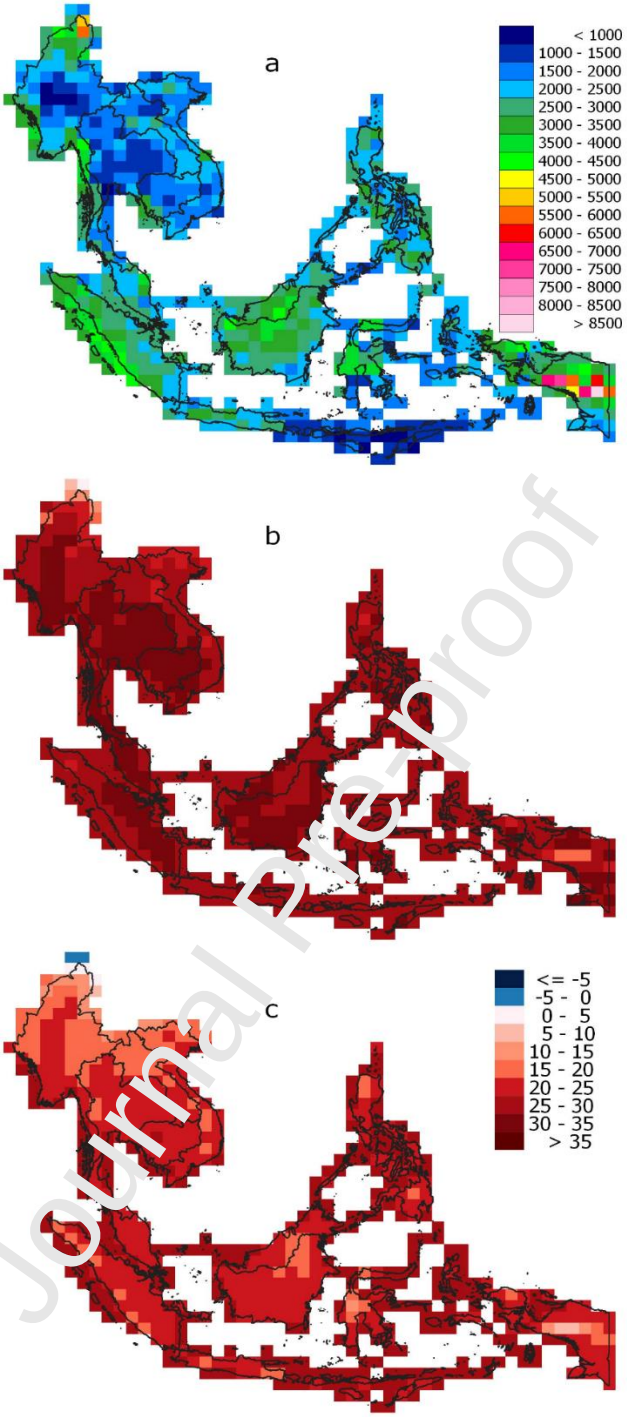

Fig. 2 Geographical distribution of long-term (1979 - 2014) (a) annual rainfall (mm), (b) mean maximum and (c) mean minimum temperatures (°C) over SEA, derived from ERA5.

2.3. CMIP6 Global Circulation Models (GCMs)

Several working groups developed historical and future CMIP6 GCMs projection (Table S1). The model results are acquired from the open-access platform (https://esgf-node.llnl.gov), which contains monthly historical (1979-2014) and future (2015-2100) rainfall, T_{max} and

T_{min}. CMIP6 offers new future scenarios, socioeconomic shared pathways (SSPs), considering the future change in earth's climate along with global economic and demographic changes, based on eight scenarios. This study investigated the future projections of the CMIP6 according to SSP 2.6, 4.5, 7.0 and 8.5 simulations. These SSPs represent a range of the lowest to highest emission scenarios and available different socioeconomic pathways. Only the first variation label, r1i1p1f1, is selected to facilitate the assessment process (Mahlstein et al., 2013). Therefore, nineteen monthly CMIP6 GCMs (historical, SSP 2.6, 4.5, 7.0 and 8.5 simulations) are employed to evaluate their ability to replicate ERA5 Köppen-Geiger climate classification over SEA and to project their future climate. Both ERA5 and GCMs are interpolated to a common grid resolution (1.0°×1.0°) to guarantee that the comparison is not biased to GCMs' spatial resolution only.

2.4. Köppen-Geiger climate classification

Wladimir Köppen was the first to introduce the Köppen climate classification scheme, followed by a modification by Wladimir Köppen and Rudolf Geiger (Köppen, 1936). It defines the world's climate zones into five primary climatic classes and 30 sub-classes based on the elements of warmth and aridity. The five primary climatic zones are delineated as A) Tropical, B) Arid, C) Temperate, D) Boreal and E) Polar. All of them are based on temperature; however arid climate zone is based on the precipitation threshold (Sanderson, 1999).

The scheme of Köppen-Geiger climate classification used in this study (Peel et al., 2007) is presented in Table S2. Climate type A (hottest) is classified according to the seasonality of rainfall as no dry season (Af), short dry season (Am) and winter dry season (Aw). Dry climate is classified as arid (BW) and semiarid (BS), while temperate and boreal climate zones are classified as no dry season (Cf or Df), winter dry (Cw or Dw) and summer dry (Cs). Finally, climate type E (coldest) is classified as tundra (ET). A detailed description of the Köppen-Geiger climate classification can be found elsewhere (Alvares et al., 2013; Cui et al., 2021a; Park et al., 2019; Peel et al., 2007).

3. Methodology

This study investigates GCMs selection based on the similarity of the Köppen-Geiger climate classification of historical observation data (ERA5) and historical CMIP6 GCMs from 1979-

2014. Fig. 3 illustrates the workflow for implementing the working procedures of this study. Rainfall, T_{max} and T_{min} are considered to classify climate according to Köppen-Geiger criteria using observed climate and each GCM. Then, the reference and simulation zoning of each GCM are compared to assess their similarity using different categorical metrics, detailed in the following sections. The GCMs in the upper rank are deemed to be mostly similar to the ERA5 Köppen-Geiger climate classification. Therefore, the best GCMs in SEA are chosen to create a multi-model ensemble (MME) that is used in the projection of climate change in the study area. The following sections detail the approaches of this work.

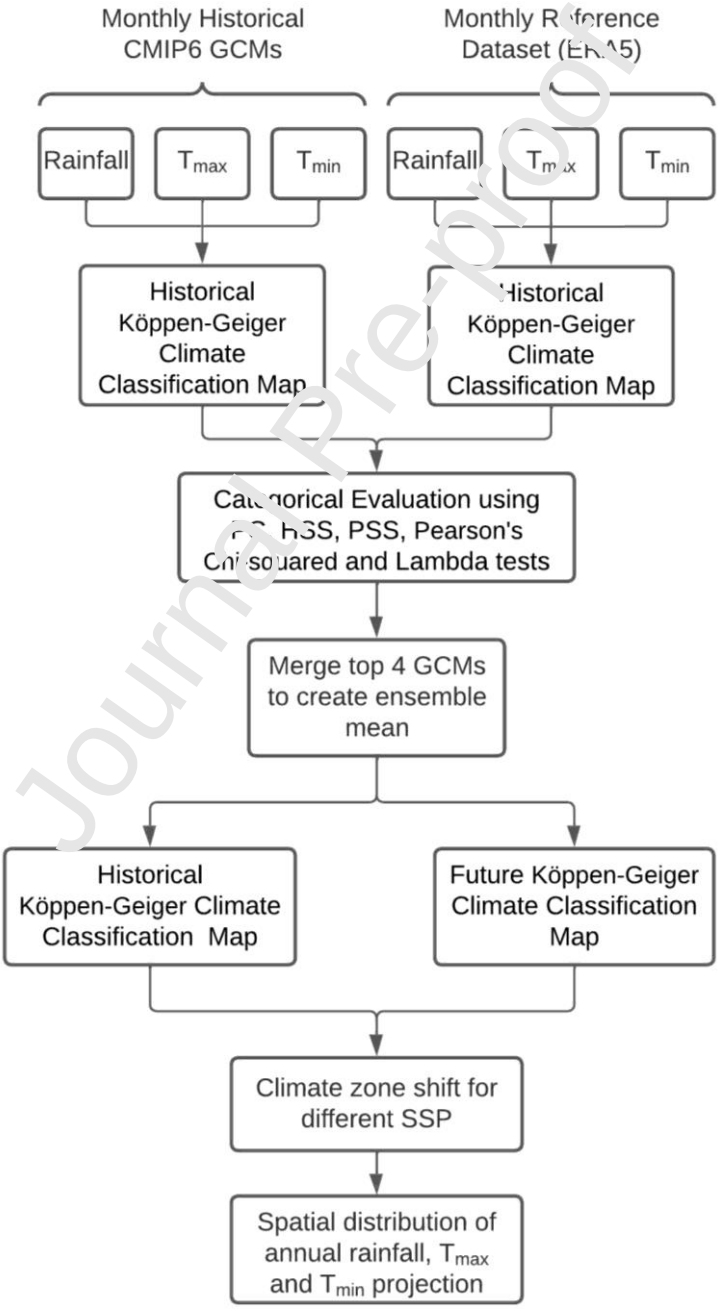

Fig. 3 Flowchart showing methodology used in this study

3.1. GCM ensemble selection

The presented study employed an approach based on five categorical evaluation metrics to assess the similarity between the reference climate zones produced using ERA5 and each GCM, Percent Correct (PC), Heidke skill score (HSS), Pierce Skill Score (PSS), Pearson's Chi-squared test and Lambda test. These metrics are based on a multi-category contingency table (Brooks and Doswell, 1996) (Table 1), which shows the frequency of the observations and estimations in different climate zone bins. In the table, $n(M_i,O_j)$ denotes the number of grids in a climate zone *i* modelled by a GCM in climate zone *j* based on ERA5 data. $n(M_i)$ represents the total number of grids in a climate zone i modelled by a GCM, whereas n(Oj) is the total number of grids originally observed in category *j*. *n* is the total number of grids, and the numbers 1 to K represent different climate zones (A1 to ET). A perfect GCM should have a non-zero value along the diagonal and zeros for other entries along the off-diagonal. The off-diagonal entries provide information about the type of bias or error in the GCM estimation of the climate zone.

The GCMs were ranked based on their performance in terms of each metric. The models ranked above 50-the percentiles or median for all indicators were finally selected. The median value was used as a threshold as the above median value indicates the better than the average performance of the models in terms of an evaluation metric.

Table 1 Multi-category contingency table

	Observed (ERA5)					
Modelled (GCM)	*i,j*	1	2	….	K	Total
	1	$n(M_1,O_1)$	$n(M_1,O_2)$	….	$n(M_1,O_k)$	$n(M_1)$
	2	$n(M_2,O_1)$	$n(M_2,O_2)$	….	$n(M_2,O_k)$	$n(M_2)$
	….	….	….	….	….	….
	K	$n(M_k,O_1)$	$n(M_k,O_2)$	….	$n(M_k,O_k)$	$n(M_k)$
	Total	$n(O_1)$	$n(O_2)$	….	$n(O_k)$	n

The PC is an intuitive metric that tells the correct estimation of climate zone fraction by a GCM compared to the reference ERA estimation Eq. (1). It ranges from 0 to 1, where 1 is a perfect score.

$$PC = \frac{1}{n}\sum_{i=1}^{k} n(Mi, Oi) \quad \text{Eq. (1)}$$

The HSS is a generalised skill score that measures the accuracy of a GCM in predicting the correct climate zone class relative to that of a random chance (Jolliffe and Stephenson, 2008) Eq. (2). It ranges between $-\infty$ to 1, where 0 denotes no skill and 1 defines a perfect score.

$$HSS = \frac{\frac{1}{n}\sum_{i=1}^{k} n(Mi, Oi) - \frac{1}{n^2}\sum_{i=1}^{k} n(Mi)n(Oi)}{1 - \frac{1}{n^2}\sum_{i=1}^{k} n(Mi)n(Oi)} \quad \text{Eq. (2)}$$

PSS is a true skill metric where the score in the numerator is the number of the correct climate class prediction, and the denominator is the fraction of the correct prediction due to random chance for unbiased predictions (Woodcock, 1976). Thus, it can provide how well a GCM can persistently estimate a correct climate class. It is expressed in Eq. (3), and like HSS, the perfect score is 1 but ranges from -1 to 1.

$$PSS = \frac{\frac{1}{n}\sum_{i=1}^{k} n(Mi, Oi) - \frac{1}{n^2}\sum_{i=1}^{k} n(Mi)n(Oi)}{1 - \frac{1}{n^2}\sum_{i=1}^{k} (n(Oi))^2} \quad \text{Eq. (3)}$$

Pearson's Chi-square statistic is used to determine if there is a significant relationship between two sets of data. The formula for determining the Chi-squared statistic is as follows:

$$x^2 = \sum \frac{(Oi - Mi)^2}{Mi} \quad \text{Eq. (4)}$$

The computed Chi-square statistic is compared to the critical value (obtained from statistical tables) for the degree of freedom (df),

$$df = (r - 1)(c - 1) \quad \text{Eq. (5)}$$

where r is the number of rows in the contingency table and c is the number of column in the contingency table.

Lambda test (λ) quantifies the correlation between nominal variables using model probabilities and provides a measure of error reduction proportionate to size in cross-tabulation research. Lambda may take on values between 0 and 1, with larger ones indicating stronger ties. Lambda test coefficient is determined as:

$$\lambda = \frac{\sum_{k=1}^{n} max_j c_{ij} - max_j \sum_{k=1}^{n} c_{ij}}{N - max_j \sum_{k=1}^{n} c_{ij}} \quad \text{Eq. (6)}$$

where c_{ij} is a contingency matrix and i and j are the groups (n) in ERA5 climate zones and GCM climate zones, respectively; max j is the maximum number of groups in the rainfall simulations.

3.2. Future projection

Potential future climatic changes in SEA are assessed by comparing CMIP6 GCM projections of annual rainfall, T_{max} and T_{min} compared to ERA5 data for the period 1979-2014. The present study separated the future into two distinct periods for in-depth analysis: the relatively close future (2020–2059) and the more distant future (2060–2099). Seasonal variability of rainfall, Tmx, and Tmn simulated by each GCM was analysed over different climatic zones. Finally, maps were generated to show the relative changes in rainfall and the absolute changes in temperature.

4. Results

4.1. Performance assessment of historical GCMs

Based on monthly rainfall, T_{max} and T_{min} of ERA5 and historical CMIP6 GCM from 1979 to 2014, Köppen-Geiger climate classification was performed over SEA. Fig. 4 represents climate classification for the historical period using ERA5 and 19 GCMs, where ERA5 estimated 10 different Köppen climate zones across the study area. The dominant climate in SEA using ERA5 was tropical without dry season (Af), covering 49% of the study area; followed by tropical with dry winter (Aw) covering 23%, tropical monsoon (Am) covering 17% and temperature dry winter and hot summer (Cwa) in 7% of total land. For mainland SEA, the dominant zone was Aw to the south and Cwa to the north, covering Myanmar and Laos. The dominant maritime SEA climate was Af, except 'Aw' in the south. The visual

identification of the difference between the derived zones using GCMs and ERA5 was very hard due to the many climate zones. Thus, three categorical evaluation metrics (PC, HSS and PSS) were used to measure consistency similarity between ERA5 and each GCM.

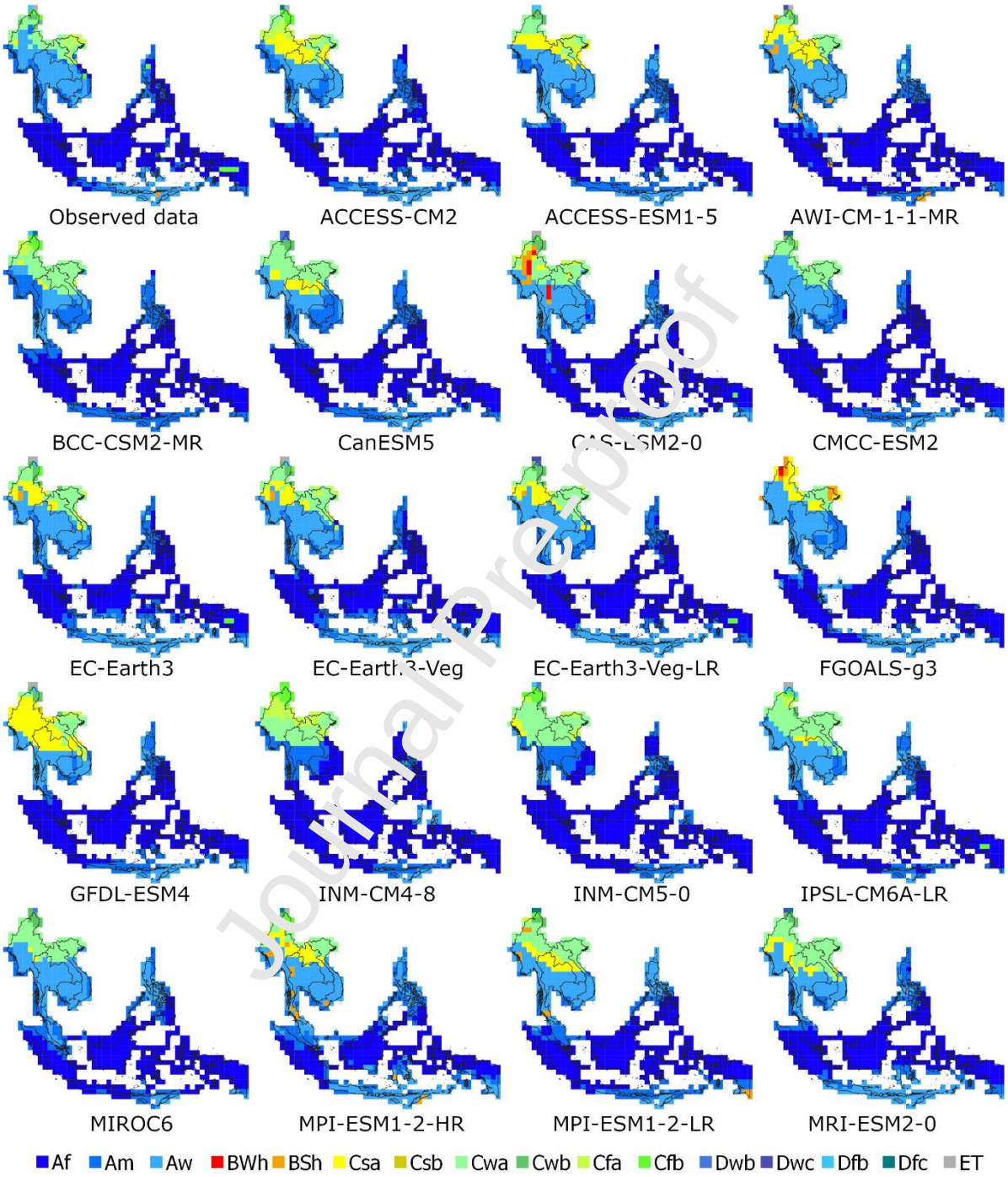

Fig. 4 Köppen-Geiger climate classification for observed data (ERA5) and 19 CMIP6 GCMs, during 1979 to 2014

A GCM with high and consistent PC, HSS, PSS and Lambda values (close to one) with the lowest chisq test results throughout the evaluation period indicates its high potential to

recreate the past Köppen-Geiger classifications. Table 2 shows the rank results obtained using five performance indicators. Most GCMs' efficiency was acceptable, except for the INM-CM4-8 and INM-CM5-0. The PCs were more than 0.55 for all GCMs, with the highest value of 0.77 for EC-Earth3-Veg. EC-Earth3-Veg showed the highest value for the other two metrics (0.68 and 0.69 for HSS and PSS, respectively), while INM-CM4-8 (0.31 for HSS and 0.29 for PSS) was the worst model in replicating Köppen-Geiger climate classification. The best-performing models above 50 percentiles in all indicators were CanESM5, CMCC-ESM2 and EC-Earth3-Veg-LR, respectively. Thus, mean MME was created from these top-ranked GCMs.

Table 2. Ranking of the GCMs according to their ability to classify the observed climate zone using PC, HSS, PSS, chisq test and Lambda test. Bold values indicate GCM's ranked above 50 percentiles in all indices.

	PC		HSS		PSS		chisq test		Lambda	
	Value	Rank	Value	Rank	Value	Rank	Value	Rank	Value	Rank
ACCESS-CM2	0.67	10	0.52	9	0.54	9	99.49	10	0.45	9
ACCESS-ESM1-5	0.69	7	0.55	7	0.56	7	102.00	13	0.46	8
AWI-CM-1-1-MR	0.63	16	0.44	15	0.44	15	91.60	6	0.37	14
BCC-CSM2-MR	0.64	13	0.47	13	0.48	13	99.49	11	0.36	15
CanESM5	**0.696**	**6**	**0.56**	**6**	**0.57**	**6**	**86.50**	**4**	**0.46**	**7**
CAS-ESM2-0	0.68	9	0.51	10	0.51	10	112.24	17	0.44	11
CMCC-ESM2	**0.748**	**4**	**0.61**	**4**	**0.59**	**4**	**88.46**	**5**	**0.53**	**4**
EC-Earth3	0.750	3	0.64	3	0.67	3	112.00	16	0.55	3
EC-Earth3-Veg	0.771	1	0.67	1	0.69	1	128.00	19	0.59	1
EC-Earth3-Veg-LR	**0.763**	**2**	**0.65**	**2**	**0.66**	**2**	**92.29**	**7**	**0.58**	**2**
FGOALS-g3	0.68	8	0.53	8	0.52	8	72.00	1	0.45	10
GFDL-ESM4	0.66	11	0.51	11	0.52	11	103.47	14	0.47	6
INM-CM4-8	0.55	19	0.30	19	0.29	19	96.00	9	0.35	17
INM-CM5-0	0.58	18	0.36	18	0.35	18	114.80	18	0.34	19
IPSL-CM6A-LR	0.63	15	0.44	16	0.43	16	80.00	2	0.35	18

MIROC6	0.65	12	0.48	12	0.48	12	84.44	3	0.35	16
MPI-ESM1-2-HR	0.58	17	0.43	17	0.46	17	103.47	15	0.40	13
MPI-ESM1-2-LR	0.63	14	0.46	14	0.48	14	94.93	8	0.40	12
MRI-ESM2-0	0.713	5	0.59	5	0.61	5	101.94	12	0.49	5

Köppen-Geiger climate classification was performed using the ensemble (Fig. 5b). The output MME was tested using the same metrics. The results showed better performance of MME in PC (0.78), HSS (0.67), PSS (0.66), chisq test (98.6) and Lambda (0.58) than individual members in most cases. Although a high similarity between the Köppen-Geiger classifications was obtained using MME and historical reference (ERA5), some differences were also noted. Some climate zones were obtained using ERA5 but not using the MME like BSh, Cfa, Dfb and ET. Overall, the major climate zones in both models were Af, Aw, Am, and Cwa.

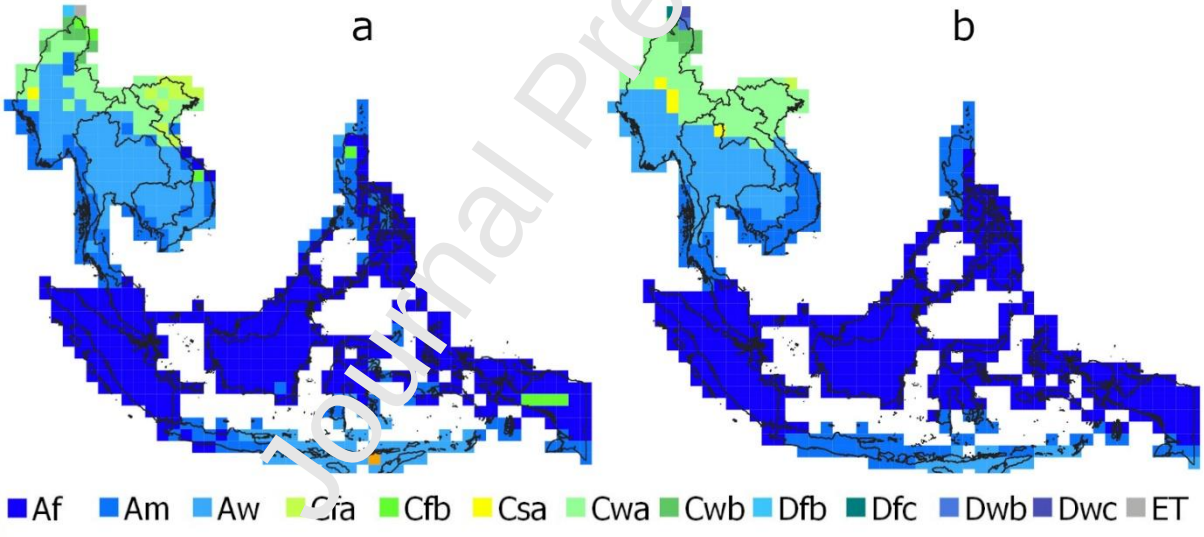

Fig. 5 Köppen-Geiger climate classification for: (a) ERA5 historical data (1979 - 2014), (b) CMIP6 historical ensemble (1979-2014)

4.2. Projections of climate zones

The MME was also used to project Köppen-Geiger climate classification, for two future periods, the near future (2020 – 2059) and far future (2060 – 2099), with respect to the base period 1979 – 2014. The classification was calculated for four SSPs and shown in Fig. 6. The projection showed 13 different climate zones in the SEA region. The climate around half of

the study area was classified as Af for all scenarios, followed by Aw, Am and Cwa. The other climate zones were covered by a small number of grids ranging between 1 and 6 grids.

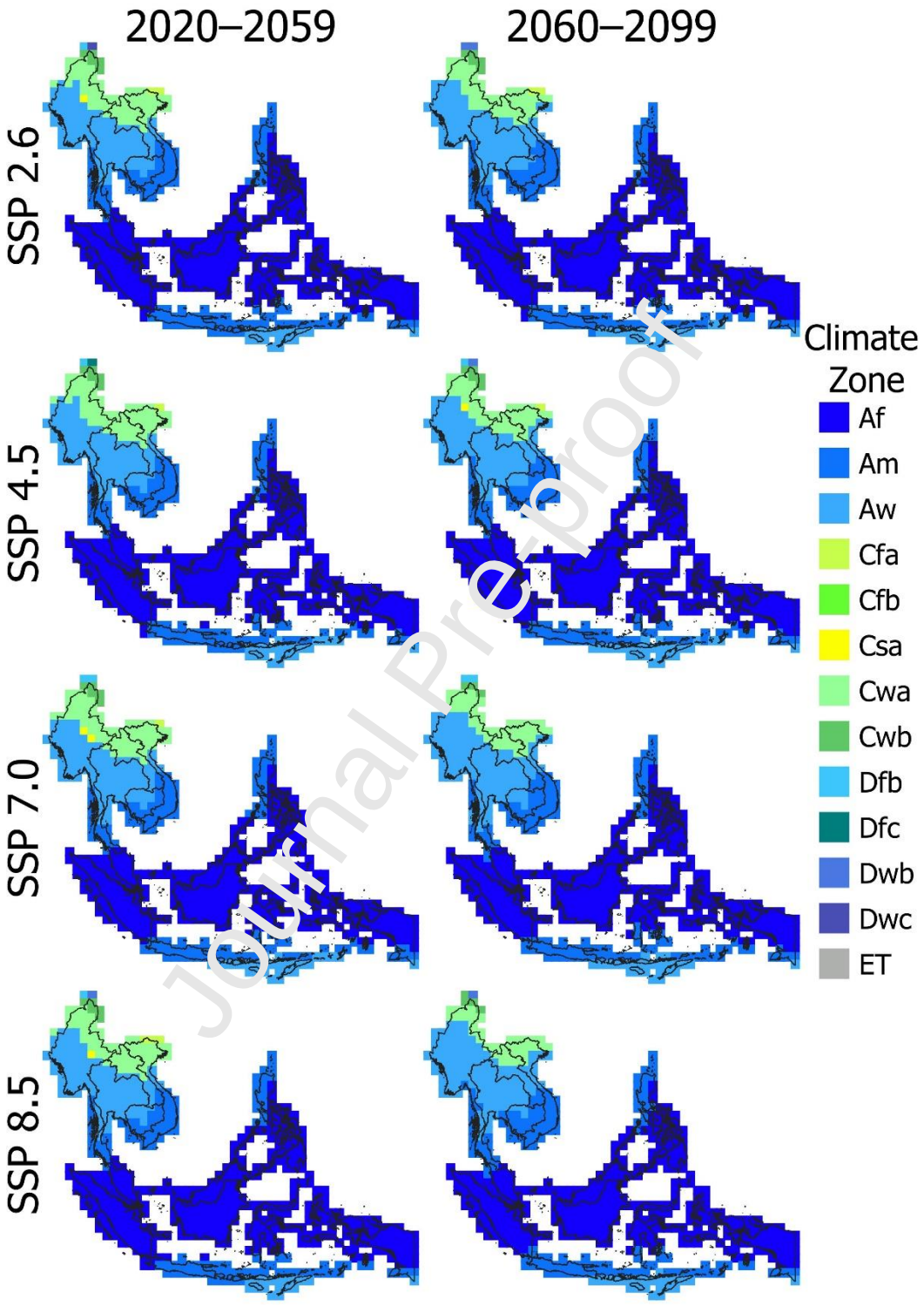

Fig. 6 Köppen-Geiger climate classification maps for SEA for two future periods (2020-2059 and 2060-2099) for four SSPs

Fig. 7 describes projected changes in Köppen-Geiger climate classification transitions during four different scenarios in the near (2020-2059) and far (2060-2099) periods over SEA. The results revealed 14 different climate transitions from one climate zone to another. Most scenarios showed a transition from temperature dry winter and hot summer (Cwa) to tropical with dry winter (Aw) in the north region, especially in the far future. This shift would happen in the north of mainland SEA. Another projected transition was from tropical with dry winter (Aw) to tropical monsoon (Am) in the south part of Vietnam, Laos and Indonesia. This transition would be mainly due to increased rainfall in the driest month. A decreased rainfall in the driest month over Banten, Indonesia, and the Philippines would cause a climate transition from tropical without dry season (Af) to tropical monsoon (Am). The central part of Myanmar would experience an increase in temperature during the coldest months, with a small increase in rainfall during the driest months. Generally, climate transition over a larger area was noticed in the far future for SSP 8.5. The climates at 82 grids were transformed from one class to another in the far future for SSP 8.5. In contrast, the climate transition over a small area was projected in the near future for SSP 4.5. The climates at only 34 grids were projected to transform in the near future for SSP 4.5. The transition in each scenario ranged from 4.9 to 12.6% of the total land area of SEA. The result indicates climate transition over a larger area in SEA for the higher emission scenario and vice-versa. A higher increase in temperature and rainfall for higher SSPs causes the transformation of more lands into different climates.

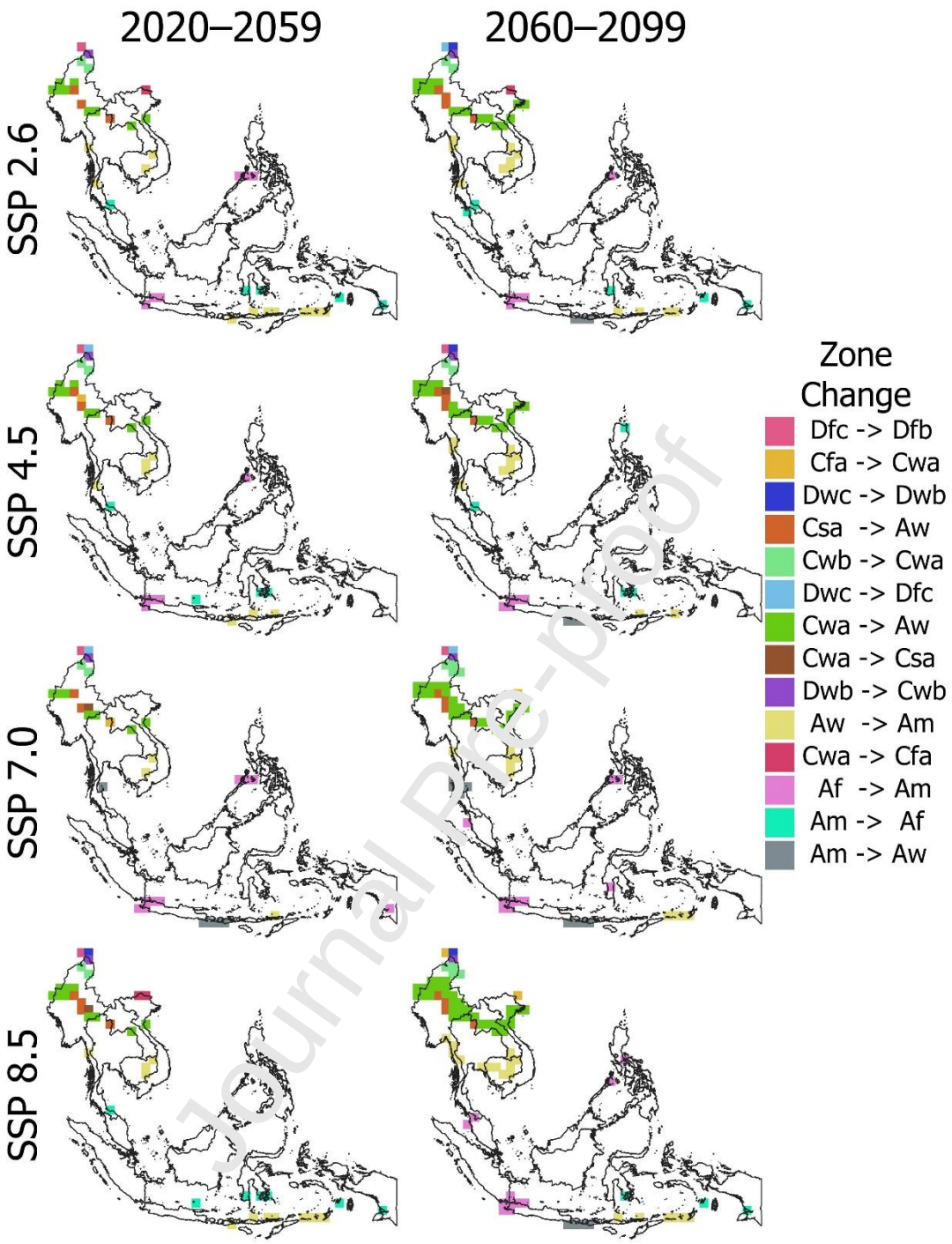

Fig. 7 Projected Köppen-Geiger climate types of transitions for SEA for two future periods (2020-2059 and 2060-2099) under four future scenarios.

The bias in estimated change (%) using each of the selected GCMs for different climate zones and future scenarios in the near and far future is presented in Fig. 8. It shows the main four different Köppen-Geiger climate zones. High positive change was projected in climate zone 'Am' for SSP 7.0 and SSP 8.5, while the lowest negative change in zone 'Af' was for the same scenarios. Cwa was the only zones that experienced a negative change for all scenarios.

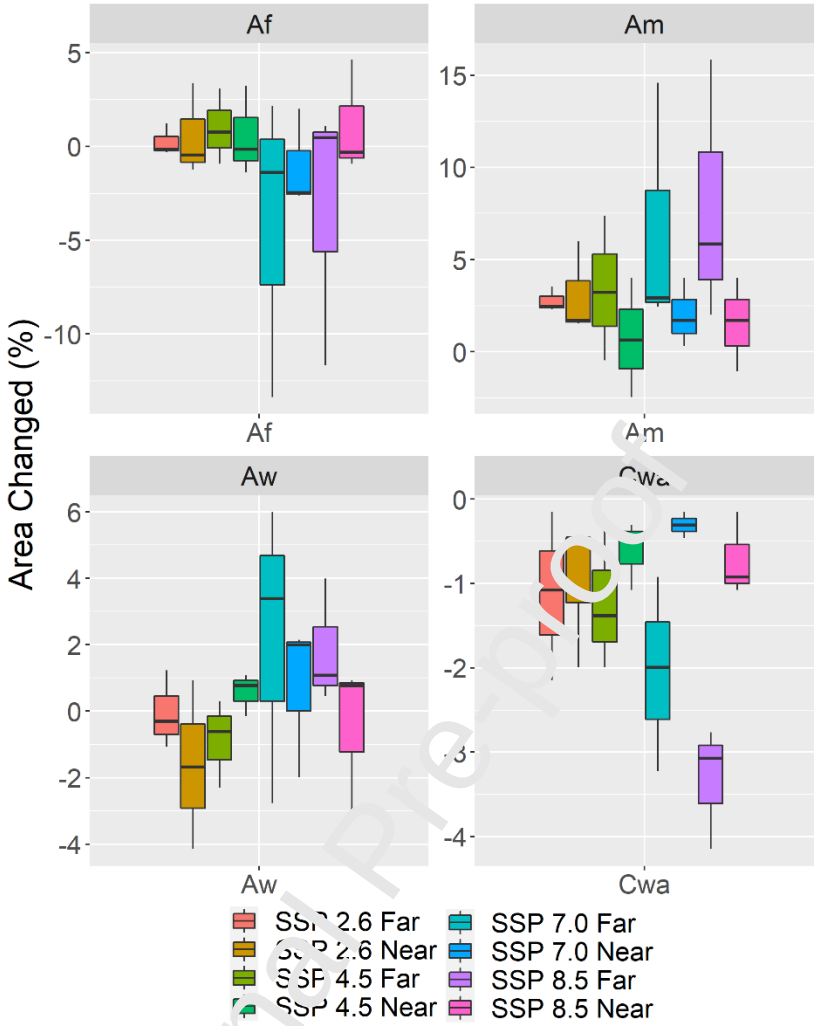

Fig. 8 Area changes in different climate zones in SEA for different future periods (near future and far future) under (SSP 2.6, 4.5, 7.0 and 8.5) scenarios based on 4 CMIP6 GCMs

The mean change in the area of different climatic zones using the MME is shown in Fig. 9. The change ranged from -2 to 2% for the near future and between -4.5 and 4% for the far future. In the near future, the highest decrease was for SSP 7.0 in climate zone Af, while in the far future, the biggest decline was in Cwa for SSP 8.5. In the far future, both Am and Aw could experience an increase of up to 4% for most of the scenarios. In contrast, Cwa might experience a decrease in all scenarios. Other climate zones would experience low or no change in both future periods.

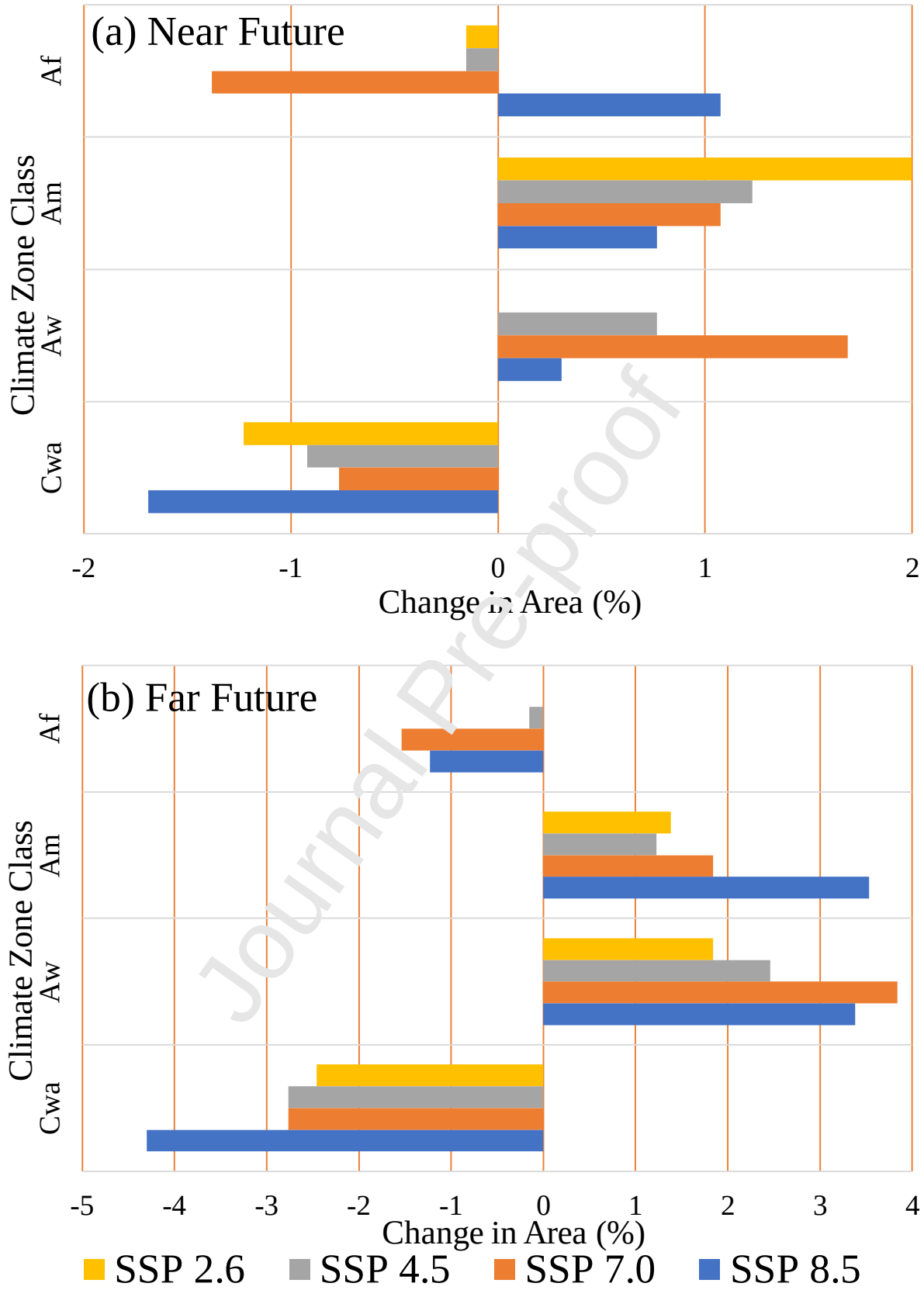

Fig. 9 Projected change in Köppen-Geiger climate zones area, derived from historical CMIP6 MME in percentage

4.3. Drivers of climate shift

Fig. 10 presents the spatial distribution of the mean MME changes in annual rainfall for SEA for different scenarios compared to the historical period (1979-2014). Similarly, Fig. 11 and Fig. ***12*** represent the mean annual absolute changes in T_{max} and T_{min}, respectively. The change in annual rainfall was between −20 and 20 %, while the changes in T_{max} and T_{min} ranged from 0 to 6 °C. For SSP 2.6 and SSP 4.5, the changes in annual rainfall ranged from -14 to 15%. The biggest change was for SSP 8.5, while the lowest was for SSP 2.6. Less than 65% of the study area would face an increase in annual rainfall, while a small region in the south and southwest would experience a decrease for all scenarios and future periods. The pattern of increase for both T_{max} and T_{min} was similar for all SSPs. SSP 2.6 showed the lowest change in both T_{max} and T_{min} (<2.0 °C), while the highest was for SSP 8.5 (>6.0 °C). A greater rise in temperature was projected in the north (>6.0 °C per decade for SSP 8.5). Due to rainfall variability over SEA, many regions were projected to shift from one climate zone to another, especially in the higher rainfall areas. For instance, projected two main shifts; one from Aw to Am due to a small increase in driest month rainfall and another from Af to Am due to a rainfall decrease in the driest month. The shift in climate due to temperature rise would be from dry winter and hot summer (Cwa) to a tropical with dry winter (Aw).

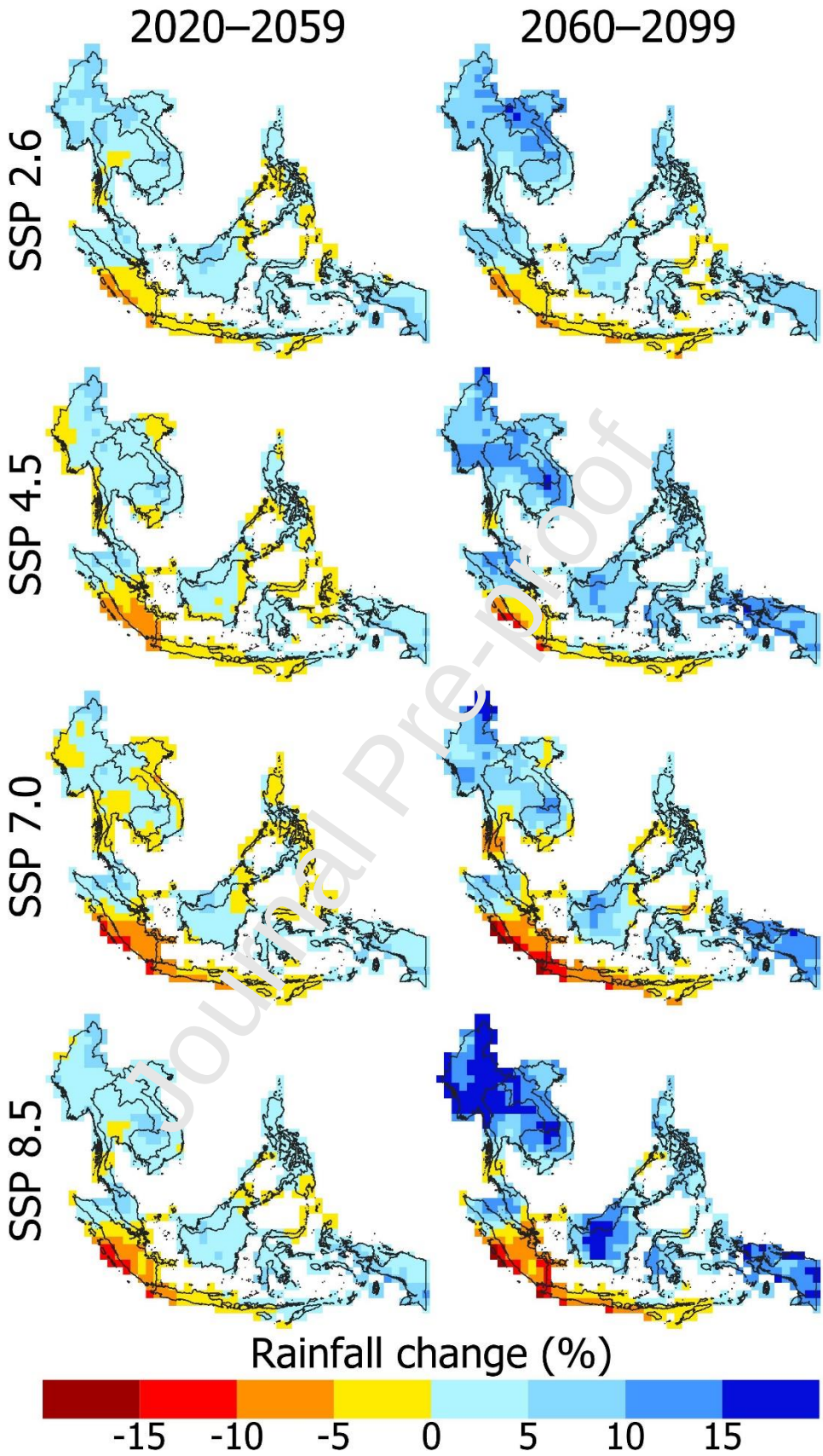

Fig. 10 Projections of annual rainfall during 2020-2059 and 2060-2099 under different SSPs.

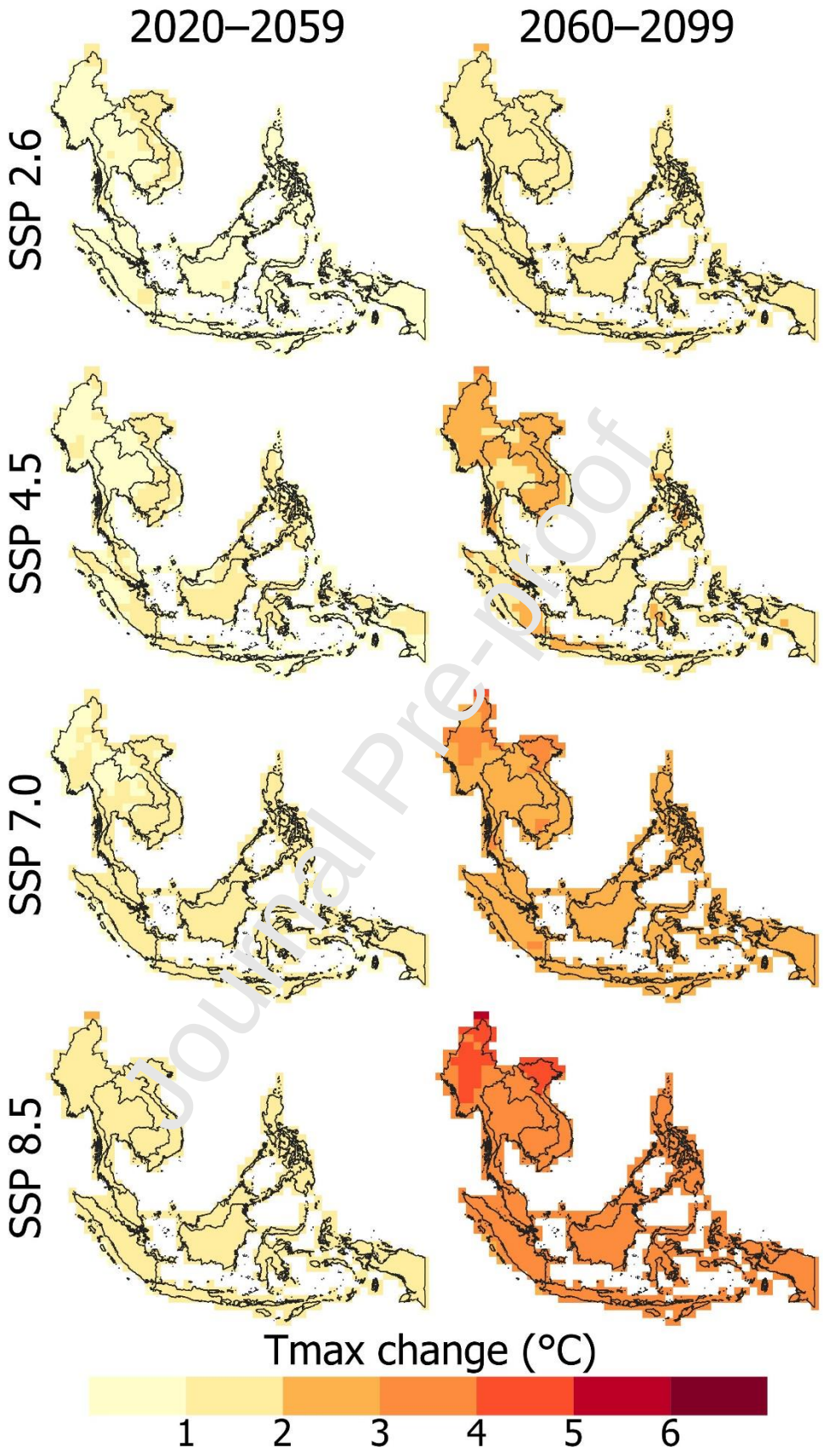

Fig. 11 Same as Fig. 10, but for Tmax.

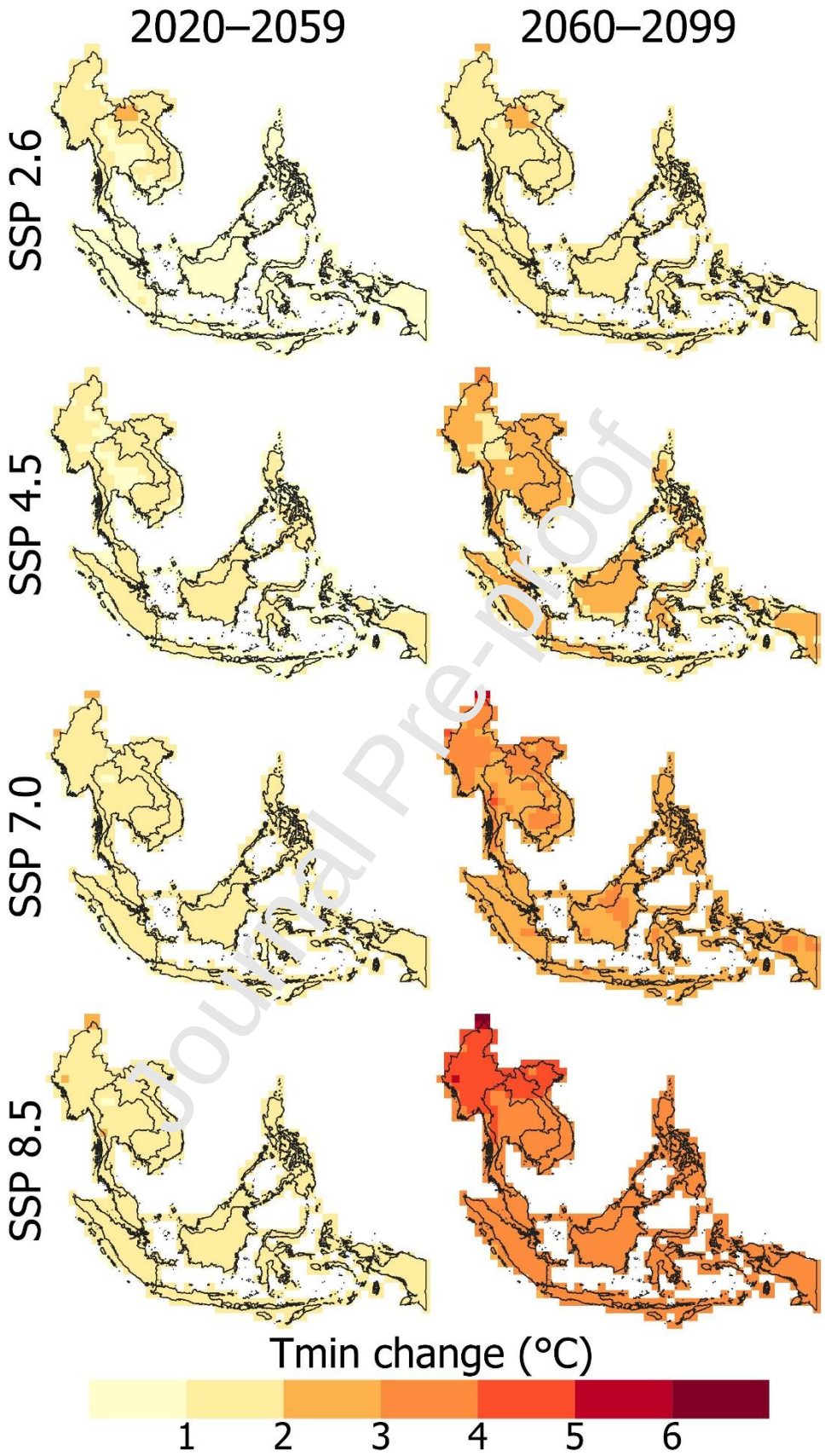

Fig. 12 Same as Fig. 10, but for Tmin.

Fig. 13 presents the seasonal variability for the three main climate shifts (Cwa to Aw, Aw to Am and Af to Am) in rainfall, T_{max} and T_{min}. The figure presents the month-to-month viability of the historical, SSP 2.6, SSP 4.5, SSP 7.0 and SSP 8.5 CMIP6 MME. Overall, all SSPs projected an increase in rainfall. The highest increase in rainfall was for SSP 8.5, while all other SSPs showed the same increase. For climate shift Aw to Am, the rainfall had the same pattern in the wet season, while the rainfall in the dry season ranged between 50 to 120 mm. Finally, the rainy season was opposite to the other two climate shifts for the transition from Af to Am. The seasonal rainfall was decreasing for almost all SSPs, except for SSP 2.6 and 4.5, which showed an increase in some months. The temperature pattern in the historical MME was similar in all climate shifts, with a similar change between SSPs. The highest temperature increase was during April and May for all SSPs. The lowest change was SSP 2.6 and the highest for SSP 8.5, indicating a higher rise in temperature for higher SSPs.

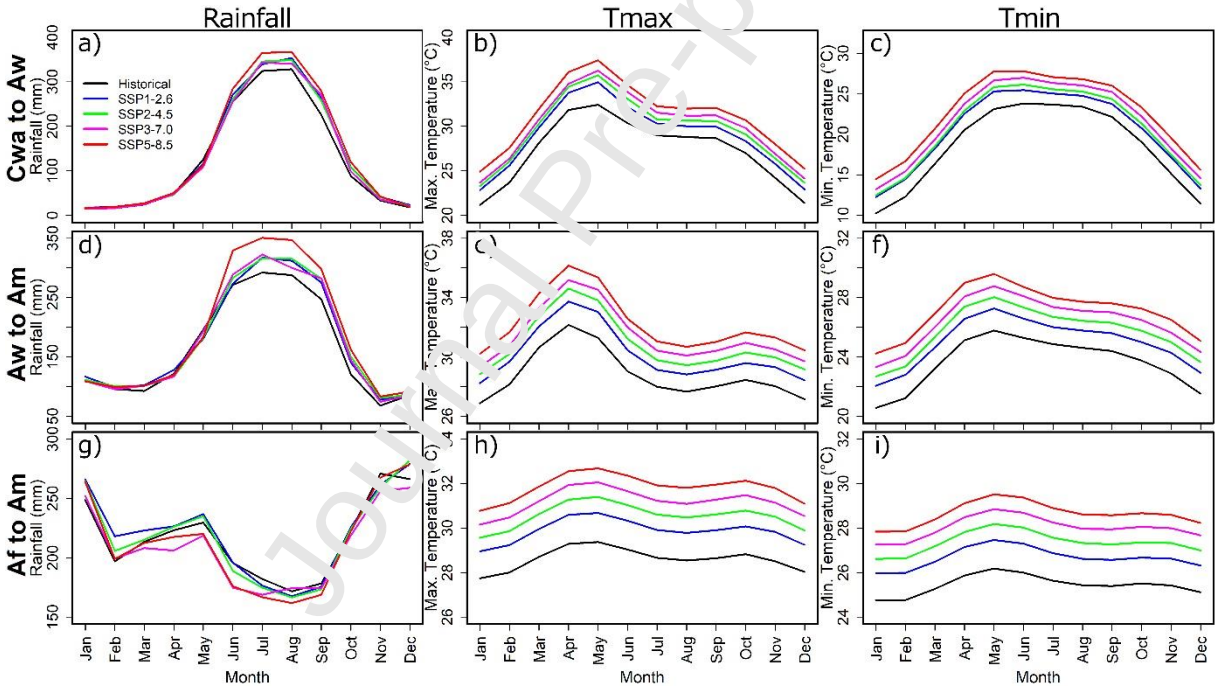

Fig. 13 Seasonal variability in (a, d and g) rainfall, (b, e and f) T_{max} and (c, f and i) T_{min} for three main climate shifts in historical and four SSPs

5. Discussion

This study evaluated possible geographical shifts in climate in SEA for different SSPs. Several studies have been conducted in different regions worldwide to compare observed and possible future shifts in climate for various climate change scenarios (Huang et al., 2016; Li et al., 2021; Rubel and Kottek, 2010; Wang et al., 2017). These studies showed a shift in

climate zones mostly in the arid and semiarid regions (Huang et al., 2016; Li et al., 2021). For example, Li et al. (2021) showed that 10.5% of the global drylands might face a climate shift for RCP8.5 scenario. Higher susceptibility of dryland to climate shift has encouraged most previous climate shift studies on arid to dry-humid regions.

The present study used three categorical evaluation metrics for GCM skill assessment. The metrics were selected as they are not dependable on the data for which they are designed (Appleman, 1960). Generally, the lack of hits causes spiky and inaccurate results in different categorical metric (Isaac et al., 2014). The metrics used in this study can overcome this drawback.

Our study is one of the few that evaluated climate shifts in humid tropical regions. Besides, all previous studies used RCPs to project future shifts in climate zones. The present study revealed that 4 to 12% of the land of SEA would experience a shift in climate for different SSPs. The shifts would be towards a more tropical or tropical monsoon for all SSPs, indicating that changes in the tropical region are opposite to those in the dry regions. The geographical coverage of dry climate is expanding in the dry region, while the geographic coverage of wet climate is increasing in the tropical region. A significant amount of land would transform from dry winter and hot summer to tropical with dry winter. It was due to an increase in the coldest month's temperature, which would cause a rise in the coldest month's mean temperature above the threshold of 18 °C. Besides, the climate over a significant amount of land would transform from tropical dry winter to tropical monsoon climate. At the same time, some regions with no dry season may experience a climate with a short dry season in the future.

The topical humid region is the most biodiverse region in the world (Sa'adi et al., 2017). It is also most vulnerable to climate change (Eguiguren-Velepucha et al., 2020). SEA has one of the dense species distributions per unit area in the world. Most of the species have a very narrow climatic niche. Climate change can severely affect biodiversity in the region. Therefore, it can be remarked that climate change may be devastating for the ecological conditions of SEA. The tropical species might experience migration and extinction (Bellard et al., 2012). Higher rainfall projected in SEA may lead to higher impermanence of dipterocarps (Deb et al., 2018). Climate change may also reduce growth rates and significantly affect crop productivity in the region.

Analysis of rainfall and temperature projection revealed that the climate of SEA is changing in line with global climate change. Temperature is rising all over SEA. However, the rise in SEA temperature is relatively less than the global average (IPCC, 2018). The present study

showed an increase in T_{max} in SEA in a range of 0.65–5.05 °C by 2100 and T_{min} by 0.63–6.30 °C. A higher increase in minimum temperature compared to maximum temperature indicates a decrease in the diurnal temperature range (DTR), suggesting the impact of high atmospheric greenhouse gas concertation in SEA. The rainfall was projected to increase and decrease in different parts of SEA. The highest increase would be in the northern SEA, up to 20% by 2100. It would also increase in most of the other parts, except in the southern region. Overall, a sharp rise in rainfall was a notable impact of climate change in SEA. The increasing rainfall pattern projected in this study using SSPs is similar to that projected for RCPs (Tangang et al., 2020). A previous study showed an increase in the average rainfall in SEA in the range of 10-20%, with a higher increase over mainland SEA and Borneo for different RCPs. The study also projected a higher increase in rainfall during wet months (December to February) like the seasonal projection of rainfall observed over the Indochina region in this study (Tangang et al., 2020).

The present study showed that although rainfall amount would increase, a large portion of land in the region would shift from monsoon-influenced humid subtropical climate to a tropical wet and dry or savanna climate. Besides, the climate in some regions with no dry season was projected to shift to a climate with a short dry season. The seasonal pattern of projected rainfall showed an increase in rainfall mostly in the high rainfall months, and no change was observed in the dry months. This would make the dry season drier than the wet season, which is consistent with other studies (Wang et al., 2014). The high seasonal rainfall variability would cause a large land to shift to drier climates within a short period. The temperature rise was noticed at the same rate for all months. The results indicated the shift in SEA climate would be mainly due to the increase in T_{min} in the north, followed by the increase in rainfall in the north and south.

Increased rainfall in the wet month would increase the probability of floods. Monsoon-driven flood is the major natural hazard in SEA. Increased frequency and severity of floods due to climate change have also been reported in Southeast Asia (Cabrera and Lee, 2018; Januriyadi et al., 2018; Mishra et al., 2018; Supharatid, 2016). Mishra et al. (2018) evaluated the impacts of climate change on floods in the Ciliwung River Basin, Jakarta, Indonesia. They projected an increase in flood inundation areas and depths ranging from 6% to 31%. Januriyadi et al. (2018) assessed flood risk for Jakarta, Indonesia, under climate change scenarios and reported a 322-402% increase in flood risk in 2050 at a significance level of 0.05. Supharatid, (2016) showed increased vulnerability to floods in Bangkok, Thailand, by nearly 100% due to

increased peak rainfall. Cabrera and Lee, (2018) reported a 50% increase in flood magnitude due to a 69% increase in rainfall intensity in Davao Oriental, Philippines. The findings of this study collaborated with previous studies.

Many researchers used ERA5 as a reference dataset for studying SEA climate (Khadka et al., 2022; Zhai et al., 2020). Khadka et al. (2022) compared four reanalysis climate datasets and showed ERA5 as the best product for SEA. It has also been found to simulate the observed climate reliably in nearby regions. Xin et al. (2021) showed ERA5 as the best product for replicating monthly rainfall in China's coastal cities and mountainous vegetation areas. Jiang et al. (2019) compared eight reanalysis datasets in Central Asia and found better performance ERA5 than others. ERA5 has some limitations, like it failed to describe the hourly and daily rainfall. This indicates uncertainty in ERA5 data representing climate at the grids with land-ocean interactions. ERA5 often underestimate the frequency of no/trace rain due to the high misdetection rate (Beck et al., 2017). It also showed some inaccuracies in describing the frequency and size of high-intensity rain at microscopic scales (Beck et al., 2017). However, the literature review indicates the overall reliability of ERA5 in climatic studies (Xin et al., 2021; Khadka et al., 2022).

The different rainfall amounts between the wet and dry seasons would lead to seasonality. The changes in precipitation patterns may influence the population distribution of species depending on the wet or dry conditions. An alteration in rainfall seasonality may also affect human comfort (Pour et al., 2020). Overall, changes in seasonality may affect land suitability for agriculture, ecology and public health in the region. The present study identified hotspots of ecologically vulnerable areas in SEA to climate change. More detailed studies with high-resolution climate projection data should be taken in the regions by considering climate shifts to mitigate the adverse impacts of climate change. Future studies can be conducted to identify necessary interventions to aid biosphere resilience to climate change in SEA or elsewhere.

6. Conclusions

A possible shift in climate zones in SEA for different SSPs and future periods was evaluated in this work through the selection of a suitable set climate model. In most regions of SEA, we found a rise in both rainfall amount and temperatures. As a result, climate shift may occur in 4 to 12% of land areas of SEA for different climate change scenarios. Overall, there will be a shift towards a more monsoon-dominated climate. The major shift would be in the northern part of SEA due to increased rainfall in the wet season. As one of the richest biodiversity

regions of the world, SEA may be severely affected by climate shifts. Ecology, agriculture and water would be the key sectors expected to be affected by the climate shift. The countries in the region need to undertake a detailed assessment of climate change in the identified hotspots of ecologically vulnerable regions to streamline their adaptation measures and development planning. In the future, the GCMs can be downscaled to a higher resolution to provide a more accurate estimation of a land shift from one to another climate zones. Besides, implications for such changes in atmospheric water balance and bioclimate can be evaluated to aid the need for climate adaptation.

Declarations

Funding

The authors are grateful to Staffordshire University, UK for providing financial support for this research through grant no. WR GCRF 2020-2021.

Conflicts of interest/Competing interests

The authors declare that they have no known competing financial interests or personal relationships that could have appeared to influence the work reported in this paper.

Code availability

The code was written using R software, R.3.4, to produce the data. The code is available upon request.

Author contributions

All authors contributed to the study conception and design. Mohammed Magdy Hamed wrote the original draft, writing - review & editing, visualisation and software. Mohamed Salem Nashwan wrote the original draft and Methodology. Shamsuddin Shahid did Conceptualization, Writing - Review & Editing and Supervision. Xiao-jun Wang did conceptualisation and supervision. Tarmizi bin Ismail did data curation, conceptualisation and supervision. Ashraf Dewan did validation and Writing - Original Draft. Md Asaduzzaman did Conceptualization and Writing - Review & Editing.

References

Ahmed, K., Sachindra, D.A., Shahid, S., Demirel, M.C., Chung, E.-S.E.S., 2019. Selection of multi-model ensemble of general circulation models for the simulation of precipitation and maximum and minimum temperature based on spatial assessment metrics. Hydrol. Earth Syst. Sci. 23, 4803–4824. https://doi.org/10.5194/hess-23-4803-2019

Almazroui, M., Saeed, F., Saeed, S., Nazrul Islam, M., Ismail, M., Klutse, N.A.B., Siddiqui, M.H., 2020. Projected Change in Temperature and Precipitation Over Africa from CMIP6. Earth Syst. Environ. 4, 455–475. https://doi.org/10.1007/s41748-020-00161-x

Alvares, C.A., Stape, J.L., Sentelhas, P.C., De Moraes Gonçalves, J.L., Sparovek, G., 2013. Köppen's climate classification map for Brazil. Meteorol. Zeitschrift 22, 711–728. https://doi.org/10.1127/0941-2948/2013/0507

Appleman, H.S., 1960. A Fallacy in the Use of Skill Scores. Bull. Am. Meteorol. Soc. 41, 64–67. https://doi.org/10.1175/1520-0477-41.2.64

Beck, H.E., Vergopolan, N., Pan, M., Levizzani, V., van Dijk, A.I.J.M., Weedon, G.P., Brocca, L., Pappenberger, F., Huffman, G.J., Wood, E.F., 2017. Global-scale evaluation of 22 precipitation datasets using gauge observations and hydrological modeling. Hydrol. Earth Syst. Sci. 21, 6201–6217. https://doi.org/10.5194/hess-21-6201-2017

Beck, H.E., Zimmermann, N.E., McVicar, T.R., Vergopolan, N., Berg, A., Wood, E.F., 2018. Present and future köppen-geiger climate classification maps at 1-km resolution. Sci. Data 5, 1–12. https://doi.org/10.1038/sdata.2018.214

Belda, M., Holtanová, E., Halenka, T., Kalvová, J., 2014. Climate classification revisited: from Köppen to Trewartha. Clim. Res. 59, 1–13.

Belda, M., Holtanová, E., Kalvová, J., Halenka, T., 2016. Global warming-induced changes in climate zones based on CMIP5 projections. Clim. Res. 71, 17–31.

Bellard, C., Bertelsmeier, C., Leadley, P., Thuiller, W., Courchamp, F., 2012. Impacts of climate change on the future of biodiversity. Ecol. Lett. 15, 365–377. https://doi.org/10.1111/j.1461-0248.2011.01736.x

Bickford, D., Howard, S.D., Ng, D.J.J., Sheridan, J.A., 2010. Impacts of climate change on the amphibians and reptiles of Southeast Asia. Biodivers. Conserv. 19, 1043–1062.

https://doi.org/10.1007/s10531-010-9782-4

Brooks, H.E., Doswell, C.A., 1996. A comparison of measures-oriented and distributions-oriented approaches to forecast verification. Weather Forecast. 11, 288–303. https://doi.org/10.1175/1520-0434(1996)011<0288:ACOMOA>2.0.CO;2

Cabrera, J.S., Lee, H.S., 2018. Impacts of Climate Change on Flood-Prone Areas in Davao Oriental, Philippines. Water . https://doi.org/10.3390/w10070893

Chen, I.-C., Hill, J.K., Ohlemüller, R., Roy, D.B., Thomas, C.D., 2011. Rapid Range Shifts of Species Associated with High Levels of Climate Warming. Science (80-.). 333, 1024 LP – 1026. https://doi.org/10.1126/science.1206432

Chhin, R., Yoden, S., 2018. Ranking CMIP5 GCMs for Model Ensemble Selection on Regional Scale : Case Study of the Indochina Region. J. Geophys. Res. Atmos. 123, 8949–8974. https://doi.org/10.1029/2017JD028026

Cui, D., Liang, S., Wang, D., 2021a. Observed and projected changes in global climate zones based on Köppen climate classification. Wiley Interdiscip. Rev. Clim. Chang. 12. https://doi.org/10.1002/wcc.701

Cui, D., Liang, S., Wang, D., Liu, Z., 2021b. Köppen-Geiger climate classification and bioclimatic variables. Earth Syst. Sci. Data 1–34.

Deb, P., Orr, A., Bromwich, D.H., Nicolas, J.P., Turner, J., Hosking, J.S., 2018. Summer Drivers of Atmospheric Variability Affecting Ice Shelf Thinning in the Amundsen Sea Embayment, West Antarctica. Geophys. Res. Lett. 45, 4124–4133. https://doi.org/10.1029/2018GL077092

Deng, X., Perkins-Kirkpatrick, S.E., Lewis, S.C., Ritchie, E.A., 2021. Evaluation of Extreme Temperatures Over Australia in the Historical Simulations of CMIP5 and CMIP6 Models. Earth's Futur. 9, e2020EF001902. https://doi.org/10.1029/2020EF001902

Eguiguren-Velepucha, P.A., Chamba, J.A.M., Mendoza, N.A.A., Ojeda-Luna, T.L., Samaniego-Rojas, N.S., Furniss, M.J., Howe, C., Mendoza, Z.H.A., 2020. Tropical ecosystems vulnerability to climate change in southern Ecuador. Trop. Conserv. Sci. 9. https://doi.org/10.1177/1940082916668007

Eyring, V., Bony, S., Meehl, G.A., Senior, C.A., Stevens, B., Stouffer, R.J., Taylor, K.E.,

2016. Overview of the Coupled Model Intercomparison Project Phase 6 (CMIP6) experimental design and organisation. Geosci. Model Dev. 9, 1937–1958. https://doi.org/10.5194/gmd-9-1937-2016

Fernandez, J.P.R., Franchito, S.H., Rao, V.B., Llopart, M., 2017. Changes in Koppen–Trewartha climate classification over South America from RegCM4 projections. Atmos. Sci. Lett. 18, 427–434. https://doi.org/10.1002/asl.785

Ge, F., Zhu, S., Peng, T., Zhao, Y., Sielmann, F., Fraedrich, K., Zhi, X., Liu, X., Tang, W., Ji, L., 2019. Risks of precipitation extremes over Southeast Asia: Does 1.5 °c or 2 °c global warming make a difference? Environ. Res. Lett. 14. https://doi.org/10.1088/1748-9326/aaff7e

Gusain, A., Ghosh, S., Karmakar, S., 2020. Added value of CMIP6 over CMIP5 models in simulating Indian summer monsoon rainfall. Atmos. Res. 232, 104680. https://doi.org/10.1016/j.atmosres.2019.104680

Hamed, K.H., 2008. Trend detection in hydrologic data: The Mann–Kendall trend test under the scaling hypothesis. J. Hydrol. 349, 350–363. https://doi.org/10.1016/j.jhydrol.2007.11.009

Hamed, M.M., Nashwan, M.S., Shahid, S., 2022. A novel selection method of CMIP6 GCMs for robust climate projections. Int. J. Climatol. 42, 4258–4272. https://doi.org/10.1002/joc.7461

Harjupa, W., Abdillah, M.R., Azura, A., Putranto, M.F., Marzuki, M., Nauval, F., Risyanto, Saufina, E., Jumiantri, N., Fathrio, I., 2022. On the utilisation of RDCA method for detecting and predicting the occurrence of heavy rainfall in Indonesia. Remote Sens. Appl. Soc. Environ. 25, 100681. https://doi.org/https://doi.org/10.1016/j.rsase.2021.100681

Harmeling, D., Eckstein, S., 2013. Global Climate Risk Index 2013. Ger. Bonn. https://doi.org/978-3-943704-04-4

Hartmann, D.L., Tank, A.M.G.K., Rusticucci, M., Alexander, L. V, Brönnimann, S., Charabi, Y.A.R., Dentener, F.J., Dlugokencky, E.J., Easterling, D.R., Kaplan, A., 2013. Observations: atmosphere and surface, in: Climate Change 2013 the Physical Science Basis: Working Group I Contribution to the Fifth Assessment Report of the

Intergovernmental Panel on Climate Change. Cambridge University Press, pp. 159–254.

Hattori, M., Mori, S., Matsumoto, J., 2011. The cross-equatorial northerly surge over the maritime continent and its relationship to precipitation patterns. J. Meteorol. Soc. Japan 89, 27–47. https://doi.org/10.2151/jmsj.2011-A02

Hersbach, H., Bell, B., Berrisford, P., Hirahara, S., Horányi, A., Muñoz-Sabater, J., Nicolas, J., Peubey, C., Radu, R., Schepers, D., Simmons, A., Soci, C., Abdalla, S., Abellan, X., Balsamo, G., Bechtold, P., Biavati, G., Bidlot, J., Bonavita, M., De Chiara, G., Dahlgren, P., Dee, D., Diamantakis, M., Dragani, R., Flemming, J., Forbes, R., Fuentes, M., Geer, A., Haimberger, L., Healy, S., Hogan, R.J., Hólm, E., Janisková, M., Keeley, S., Laloyaux, P., Lopez, P., Lupu, C., Radnoti, G., de Rosnay, P., Rozum, I., Vamborg, F., Villaume, S., Thépaut, J.-N., 2020. The ERA5 global reanalysis. Q. J. R. Meteorol. Soc. 146, 1999–2049. https://doi.org/10.1002/qj.3803

Holbourn, A.E., Kuhnt, W., Clemens, S.C., Kochhann, K.G.D., Jöhnck, J., Lübbers, J., Andersen, N., 2018. Late Miocene climate cooling and intensification of southeast Asian winter monsoon. Nat. Commun. 9, 1584. https://doi.org/10.1038/s41467-018-03950-1

Holdridge, L.R., 1947. Determination of world plant formations from simple climatic data. Science (80-.). 105, 367–368.

Huang, J., Yu, H., Guan, X., Wang, G., Guo, R., 2016. Accelerated dryland expansion under climate change. Nat. Clim. Chang. 6, 166–171. https://doi.org/10.1038/nclimate2837

Hubalek, Z., Horakova, M., 1988. Evaluation of Climatic Similarity Between Areas in Biogeography. J. Biogeogr. 15, 409–418. https://doi.org/10.2307/2845272

Iliopoulou, T., Papalexiou, S.M., Markonis, Y., Koutsoyiannis, D., 2018. Revisiting long-range dependence in annual precipitation. J. Hydrol. 556, 891–900. https://doi.org/https://doi.org/10.1016/j.jhydrol.2016.04.015

IPCC, 2018. IPCC SR15: Summary for Policymakers, in: IPCC Special Report Global Warming of 1.5 °C. Intergovernmental Panel on Climate Change.

IPCC, 2007. Climate Change 2007 - The Physical Science Basis: Working Group I Contribution to the Fourth Assessment Report of the IPCC, Science. https://doi.org/volume

Isaac, G.A., Bailey, M., Boudala, F.S., Burrows, W.R., Cober, S.G., Crawford, R.W., Donaldson, N., Gultepe, I., Hansen, B., Heckman, I., Huang, L.X., Ling, A., Mailhot, J., Milbrandt, J.A., Reid, J., Fournier, M., 2014. The Canadian Airport Nowcasting System (CAN-Now). Meteorol. Appl. 21, 30–49. https://doi.org/https://doi.org/10.1002/met.1342

Januriyadi, F.N., Kazama, S., Riyando Moe, I., Kure, S., 2018. Evaluation of future flood risk in Asian megacities: a case study of Jakarta. Hydrol. Res. Lett. 12, 14–22. https://doi.org/10.3178/hrl.12.14

Jiang, J., Zhou, T., Zhang, W., 2019. Evaluation of Satellite and Reanalysis Precipitable Water Vapor Data Sets Against Radiosonde Observations in Central Asia. Earth Sp. Sci. 6, 1129–1148. https://doi.org/10.1029/2019EA000651

Jiang, X., Waliser, D.E., Xavier, P.K., Petch, J., Klingaman, N.P., Woolnough, S.J., Guan, B., Bellon, G., Crueger, T., DeMott, C., Hannay, C., Lin, H., Hu, W., Kim, D., Lappen, C.-L., Lu, M.-M., Ma, H.-Y., Miyakawa, T., Kinter, J.A., Schubert, S.D., Scinocca, J., Seo, K.-H., Shindo, E., Song, X., Stan, C., Tseng, W.-L., Wang, W., Wu, T., Wu, X., Wyser, K., Zhang, G.J., Zhu, H., 2015. Vertical structure and physical processes of the Madden-Julian oscillation : exploring key model physics in climate simulations. J. Geophys. Res. Atmos. 120, 4718–4748. https://doi.org/10.1002/ 2014JD022375

Jolliffe, I.T., Stephenson, D.B., 2008. Proper scores for probability forecasts can never be equitable. Mon. Weather Rev. 136, 1505–1510. https://doi.org/10.1175/2007MWR2194.1

Karl, T.R., Melillo, J.M., Peterson, T.C., Hassol, S.J., 2009. Global climate change impacts in the United States. Cambridge University Press.

Khadka, D., Babel, M.S., Abatan, A.A., Collins, M., 2022. An evaluation of CMIP5 and CMIP6 climate models in simulating summer rainfall in the Southeast Asian monsoon domain. Int. J. Climatol. 42, 1181–1202. https://doi.org/10.1002/joc.7296

Kim, J.-B., Bae, D.-H., 2021. The Impacts of Global Warming on Climate Zone Changes Over Asia Based on CMIP6 Projections. Earth Sp. Sci. 8, e2021EA001701. https://doi.org/10.1029/2021EA001701

Knutti, R., Furrer, R., Tebaldi, C., Cermak, J., Meehl, G.A., 2010. Challenges in combining

projections from multiple climate models. J. Clim. 23, 2739–2758. https://doi.org/10.1175/2009JCLI3361.1

Köppen, W.P., 1936. Das geographische System der Klimate: Mit 14 Textfiguren. Borntraeger. https://doi.org/10.2307/200498

Kottek, M., Grieser, J., Beck, C., Rudolf, B., Rubel, F., 2006. World map of the Köppen-Geiger climate classification updated. Meteorol. Zeitschrift 15, 259–263. https://doi.org/10.1127/0941-2948/2006/0130

Kriticos, D.J., Webber, B.L., Leriche, A., Ota, N., Macadam, I., Bathols, J., Scott, J.K., 2012. CliMond: Global high-resolution historical and future scenario climate surfaces for bioclimatic modelling. Methods Ecol. Evol. 3, 53–64. https://doi.org/10.1111/j.2041-210X.2011.00134.x

Kuo, C.-C., Gan, T.Y., Wang, J., 2020. Climate change impact to Mackenzie river Basin projected by a regional climate model. Clim. Dyn. 54, 3561–3581. https://doi.org/10.1007/s00382-020-05177-7

Li, M., Wu, P., Sexton, D.M.H., Ma, Z., 2021. Potential shifts in climate zones under a future global warming scenario using soil moisture classification. Clim. Dyn. 56, 2071–2092. https://doi.org/10.1007/s00382-020-05576-w

Li, P., Feng, Z., Jiang, L., Liao, C., Zhang, J., 2014. A Review of Swidden Agriculture in Southeast Asia. Remote Sens. . https://doi.org/10.3390/rs6021654

Loarie, S.R., Duffy, P.B., Hamilton, H., Asner, G.P., Field, C.B., Ackerly, D.D., 2009. The velocity of climate change. Nature 462, 1052–1055. https://doi.org/10.1038/nature08649

Lobell, D.B., Gourdji, S.M., 2012. The Influence of Climate Change on Global Crop Productivity. Plant Physiol. 160, 1686–1697. https://doi.org/10.1104/pp.112.208298

Lutz, A.F., ter Maat, H.W., Biemans, H., Shrestha, A.B., Wester, P., Immerzeel, W.W., 2016. Selecting representative climate models for climate change impact studies: an advanced envelope-based selection approach. Int. J. Climatol. 36, 3988–4005. https://doi.org/10.1002/joc.4608

Mahlstein, I., Daniel, J.S., Solomon, S., 2013. Pace of shifts in climate regions increases with global temperature. Nat. Clim. Chang. 3, 739–743. https://doi.org/10.1038/nclimate1876

Mishra, B.K., Rafiei Emam, A., Masago, Y., Kumar, P., Regmi, R.K., Fukushi, K., 2018. Assessment of future flood inundations under climate and land use change scenarios in the Ciliwung River Basin, Jakarta. J. Flood Risk Manag. 11, S1105–S1115. https://doi.org/https://doi.org/10.1111/jfr3.12311

Moss, R.H., Edmonds, J.A., Hibbard, K.A., Manning, M.R., Rose, S.K., van Vuuren, D.P., Carter, T.R., Emori, S., Kainuma, M., Kram, T., Meehl, G.A., Mitchell, J.F.B., Nakicenovic, N., Riahi, K., Smith, S.J., Stouffer, R.J., Thomson, A.M., Weyant, J.P., Wilbanks, T.J., 2010. The next generation of scenarios for climate change research and assessment. Nature 463, 747–756. https://doi.org/10.1038/nature08823

Mukherjee, S., Mishra, A., Trenberth, K.E., 2018. Climate Change and Drought: a Perspective on Drought Indices. Curr. Clim. Chang. Reports 4, 145–163. https://doi.org/10.1007/s40641-018-0098-x

Nasional, B.P.P., 2012. National Action Plan for Climate Change Adaptation (RAN-API), Jakarta: Bappenas.

Netzel, P., Stepinski, T., 2016. On using a clustering approach for global climate classification. J. Clim. 29, 3387–3401. https://doi.org/10.1175/JCLI-D-15-0640.1

Netzel, P., Stepinski, T.F., 2017. World Climate Search and Classification Using a Dynamic Time Warping Similarity Function BT - Advances in Geocomputation. Adv. Geocomputation 181–195.

Ombadi, M., Nguyen, P., Sorooshian, S., Hsua, K., 2020. Retrospective Analysis and Bayesian Model Averaging of CMIP6 Precipitation in the Nile River Basin. J. Hydrometeorol. https://doi.org/10.1175/jhm-d-20-0157.1

Park, S., Park, H., Im, J., Yoo, C., Rhee, J., Lee, B., Kwon, C.G., 2019. Delineation of high resolution climate regions over the Korean Peninsula using machine learning approaches. PLoS One 14, 1–23. https://doi.org/10.1371/journal.pone.0223362

Parmesan, C., 2006. Ecological and Evolutionary Responses to Recent Climate Change. Annu. Rev. Ecol. Evol. Syst. 37, 637–669. https://doi.org/10.1146/annurev.ecolsys.37.091305.110100

Peel, M.C., Finlayson, B.L., McMahon, T.A., 2007. Updated world map of the Köppen-

Geiger climate classificatio. Hydrol. Earth Syst. Sci. 11, 1633–1644. https://doi.org/10.1002/ppp.421

Pour, S.H., Wahab, A.K.A., Shahid, S., 2020. Spatiotemporal changes in precipitation indicators related to bioclimate in Iran. Theor. Appl. Climatol. 141, 99–115. https://doi.org/10.1007/s00704-020-03192-6

Raitzer, D., Bosello, F., Tavoni, M., Orecchia, C., Marangoni, G., Samson, J., 2015. Southeast Asia and the economics of global climate stabilisation. Asian Dev. Bank.

Robertson, A.W., Moron, V., Qian, J.H., Chang, C.P., Tangang, F., Aldrian, E., Koh, T.Y., Juneng, L., 2011. The Maritime Continent Monsoon, in: Global Monsoon System, The: Research and Forecast, 2nd Edition, World Scientific Series on Asia-Pacific Weather and Climate. WORLD SCIENTIFIC, pp. 85–98. https://doi.org/10.1142/9789814343411_0006

Rohli, R. V, Andrew Joyner, T., Reynolds, S.J., Shaw, C., Vázquez, J.R., 2015. Globally Extended Köppen–Geiger climate classification and temporal shifts in terrestrial climatic types. Phys. Geogr. 36, 142–157. https://doi.org/10.1080/02723646.2015.1016382

Rubel, F., Kottek, M., 2010. Observed and projected climate shifts 1901-2100 depicted by world maps of the Köppen-Geiger climate classification. Meteorol. Zeitschrift 19, 135–141. https://doi.org/10.1127/0941-2948/2010/0430

Sa'adi, Z., Shahid, S., Chung, E.S., Ismail, T. bin, 2017. Projection of spatial and temporal changes of rainfall in Sarawak of Borneo Island using statistical downscaling of CMIP5 models. Atmos. Res. 197, 446–460. https://doi.org/10.1016/j.atmosres.2017.08.002

Salehie, O., Hamed, M.M., Ismail, T., Tam, T.H., Shahid, S., 2021. Selection of CMIP6 GCM With Projection of Climate Over The Amu Darya River Basin. Prepr. (Version 1) available Res. Sq. 1–27. https://doi.org/10.21203/rs.3.rs-1031530/v1

Sanderson, M., 1999. The Classification of Climates from Pythagoras to Koeppen. Bull. Am. Meteorol. Soc. 80, 669–673. https://doi.org/10.1175/1520-0477(1999)080<0669:TCOCFP>2.0.CO;2

Schlund, M., Lauer, A., Gentine, P., Sherwood, S.C., Eyring, V., 2020. Emergent constraints

on Equilibrium Climate Sensitivity in CMIP5 : do they hold for CMIP6 ? Earth Syst. Dyn. 1–40. https://doi.org/10.5194/esd-2020-49

Sen, P.K., 1968. Estimates of the Regression Coefficient Based on Kendall's Tau. J. Am. Stat. Assoc. 63, 1379–1389. https://doi.org/10.1080/01621459.1968.10480934

Supharatid, S., 2016. Skill of precipitation projectionin the Chao Phraya river Basinby multi-model ensemble CMIP3-CMIP5. Weather Clim. Extrem. 12, 1–14. https://doi.org/https://doi.org/10.1016/j.wace.2016.03.001

Supharatid, S., Nafung, J., 2021. Projected drought conditions by CMIP6 multimodel ensemble over Southeast Asia. J. Water Clim. Chang. 12, 3330–3354. https://doi.org/10.2166/wcc.2021.308

Tangang, F., Chung, J.X., Juneng, L., Supari, Salimun, E., Ngai, S.T., Jamaluddin, A.F., Mohd, M.S.F., Cruz, F., Narisma, G., Santisirisomboon, J., Ngo-Duc, T., Van Tan, P., Singhruck, P., Gunawan, D., Aldrian, E., Sopaheluwakan, A., Grigory, N., Remedio, A.R.C., Sein, D. V., Hein-Griggs, D., McGregor, J.L., Yang, H., Sasaki, H., Kumar, P., 2020. Projected future changes in rainfall in Southeast Asia based on CORDEX–SEA multi-model simulations. Clim. Dyn. 55, 1247–1267. https://doi.org/10.1007/s00382-020-05322-2

Taylor, K.E., Stouffer, R.J., Meehl, G.A., 2012. An overview of CMIP5 and the experiment design. Bull. Am. Meteorol. Soc. 93, 485–498. https://doi.org/10.1175/BAMS-D-11-00094.1

Taylor, R.G., Scanlon, B., Döll, P., Rodell, M., van Beek, R., Wada, Y., Longuevergne, L., Leblanc, M., Famiglietti, J.S., Edmunds, M., Konikow, L., Green, T.R., Chen, J., Taniguchi, M., Bierkens, M.F.P., MacDonald, A., Fan, Y., Maxwell, R.M., Yechieli, Y., Gurdak, J.J., Allen, D.M., Shamsudduha, M., Hiscock, K., Yeh, P.J.-F., Holman, I., Treidel, H., 2013. Ground water and climate change. Nat. Clim. Chang. 3, 322–329. https://doi.org/10.1038/nclimate1744

Tebaldi, C., Knutti, R., 2007. The use of the multi-model ensemble in probabilistic climate projections. Philos. Trans. R. Soc. A Math. Phys. Eng. Sci. 365, 2053–2075. https://doi.org/10.1098/rsta.2007.2076

Tomaszkiewicz, M.A., 2021. Future seasonal drought conditions over the cordex-mena/arab

domain. Atmosphere (Basel). 12. https://doi.org/10.3390/atmos12070856

Valentin, C., Agus, F., Alamban, R., Boosaner, A., Bricquet, J.P., Chaplot, V., de Guzman, T., de Rouw, A., Janeau, J.L., Orange, D., Phachomphonh, K., Do Duy Phai, Podwojewski, P., Ribolzi, O., Silvera, N., Subagyono, K., Thiébaux, J.P., Tran Duc Toan, Vadari, T., 2008. Runoff and sediment losses from 27 upland catchments in Southeast Asia: Impact of rapid land use changes and conservation practices. Agric. Ecosyst. Environ. 128, 225–238. https://doi.org/https://doi.org/10.1016/j.agee.2008.06.004

Vinke, K., Schellnhuber, H.J., Coumou, D., Geiger, T., Glanemann, N., Huber, V., Kropp, J.P., Kriewald, S., Lehmann, J., Levermann, A., Lobanova, A., Knaus, M., Otto, C., Reyer, C., Robinson, A., Rybski, D., Schewe, J., Wilner, S., Wortmann, M., Zhao, F., Zhou, B., Laplante, B., Lu, X., Rodgers, C., 2017. A Region at Risk: The Human Dimensions of Climate Change in Asia and the Pacific. A Reg. Risk Hum. Dimens. Clim. Chang. Asia Pacific. https://doi.org/http://dx.doi.org/10.22617/TCS178839-2

Walter, S.D., Elwood, J.M., 1975. A test for seasonality of events with a variable population at risk. Br. J. Prev. & Soc. Med. 29, 18 LP – 21. https://doi.org/10.1136/jech.29.1.18

Wang, X., Huang, G., Liu, J., 2014. Projected increases in intensity and frequency of rainfall extremes through a regional climate modeling approach. J. Geophys. Res. Atmos. 119, 13,213-271,286. https://doi.org/https://doi.org/10.1002/2014JD022564

Wang, Z., Lin, L., Zhang, Y., Zhang, H., Liu, L., Xu, Y., 2017. Scenario dependence of future changes in climate extremes under 1.5 °C and 2 °C global warming. Sci. Rep. 7, 46432. https://doi.org/10.1038/srep46432

Weigel, A.P., Knutti, R., Liniger, M.A., Appenzeller, C., 2010. Risks of model weighting in multimodel climate projections. J. Clim. 23, 4175–4191. https://doi.org/10.1175/2010JCLI3594.1

Williams, J.W., Jackson, S.T., Kutzbach, J.E., 2007. Projected distributions of novel and disappearing climates by 2100 AD. Proc. Natl. Acad. Sci. 104, 5738 LP – 5742. https://doi.org/10.1073/pnas.0606292104

Woetzel, J., Pinner, D., Samandari, H., 2020. Climate Risk and response. McKinsey Global

Institute.

Woodcock, F., 1976. The Evaluation of Yes/No Forecasts for Scientific and Administrative Purposes. Mon. Weather Rev. 104, 1209–1214. https://doi.org/10.1175/1520-0493(1976)104<1209:TEOYFF>2.0.CO;2

Xavier, P., Rahmat, R., Cheong, W.K., Wallace, E., 2014. Influence of Madden-Julian Oscillation on Southeast Asia rainfall extremes: Observations and predictability. Geophys. Res. Lett. 41, 4406–4412. https://doi.org/https://doi.org/10.1002/2014GL060241

Xin, Y., Lu, N., Jiang, H., Liu, Y., Yao, L., 2021. Performance of ERA5 reanalysis precipitation products in the Guangdong-Hong Kong-Macao greater Bay Area, China. J. Hydrol. 602, 126791. https://doi.org/10.1016/j.jhydrol.2021.126791

Yang, S., Wu, R., Jian, M., Huang, J., Hu, X., Wang, Z., Jiang, X., 2021. Climate Change in Southeast Asia and Surrounding Areas, Springer Climate. Springer Climate.

Zhai, J., Mondal, S.K., Fischer, T., Wang, Y., Su, B., Huang, J., Tao, H., Wang, G., Ullah, W., Uddin, M.J., 2020. Future drought characteristics through a multi-model ensemble from CMIP6 over South Asia. Atmos. Res. 246, 105111. https://doi.org/10.1016/j.atmosres.2020.105111

Zhang, X., Cai, X., 2013. Climate change impacts on global agricultural water deficit. Geophys. Res. Lett. 40, 1111–1117. https://doi.org/https://doi.org/10.1002/grl.50279

Zhao, S., Peng, C., Jiang, H., Tian, D., Lei, X., Zhou, X., 2006. Land use change in Asia and the ecological consequences. Ecol. Res. 21, 890–896. https://doi.org/10.1007/s11284-006-0048-2

All authors contributed to the study conception and design. Mohammed Magdy Hamed wrote the original draft, writing - review & editing, visualization and software. Mohamed Salem Nashwan wrote the original draft and Methodology. Shamsuddin Shahid did Conceptualization, Writing - Review & Editing and Supervision. Xiao-jun Wang did conceptualization and supervision. Tarmizi bin Ismail did data curation, conceptualization and supervision. Ashraf Dewan did validation and Writing - Original Draft. Md Asaduzzaman did Conceptualization and Writing - Review & Editing.